J. Fluid Mech. (1976), *vol.* 76, *part* 3, *pp.* 519–559
Printed in Great Britain

Pressure and force distributions on a sharp-nosed circular cylinder at large angles of inclination to a uniform subsonic stream

By P. J. LAMONT AND B. L. HUNT
Department of Aeronautical Engineering, University of Bristol, England

(Received 27 October 1975)

This paper reports an experimental investigation of pressure and force distributions on a sharp-nosed circular cylinder inclined to a uniform low-speed air flow under conditions of laminar separation of the boundary layer. The main concern is with the out-of-plane force (i.e. the side force if the body is at incidence). The experimental model consisted of an extensively pressure-tapped cylinder to which four different noses were fitted. The results show that there is an oscillatory distribution of out-of-plane force along the cylinder for most of the inclination range 0–90°. The amplitude of this distribution is strongly affected by nose shape in conditions where the out-of-plane force extends onto the nose. At very high angles of inclination the oscillatory distribution disappears and is replaced by a vortex pattern like that found on an infinite yawed cylinder. The general nature of the out-of-plane force is found to be consistent with the impulsively started flow analogy. Unsteadiness in the flow was found to cause a serious reduction in many of the time-averaged values. The unsteadiness is ascribed to the switching of the flow pattern due to free-stream turbulence. Measurements of the time histories of certain pressures enabled values of the force in the unswitched state to be calculated. The Reynolds number was found to have an important influence at inclinations above 55°. However, it was also found that the range of Reynolds numbers over which this effect occurs can depend on the scale of the model.

1. Introduction

When a slender body is inclined to an air stream it experiences components of force in the plane in which the inclination occurs and a component perpendicular to that plane. These forces have received various names in the literature arising from whether the inclination has taken place in the horizontal or in the vertical plane. For an axisymmetric body there is no aerodynamic significance in the orientation of the plane of inclination; we shall therefore follow our previous practice (Lamont & Hunt 1973) and refer to the components as in-plane and out-of-plane forces respectively. The in-plane force can be conveniently resolved in turn into a component which is perpendicular to the axis of the body (called here the in-plane normal force) and a component parallel to the axis (called the in-plane axial force in our terminology).

The measurement and prediction of these forces has been of interest for a number of years. The earlier work was mainly concerned with the in-plane normal force because this exists at low inclinations and can be large over the nose region. Munk (1924) was one of the first to study the problem and he introduced the cross-flow approach, which has been the basis of all in-plane normal force prediction methods. Munk's work was concerned with an ideal fluid and only relevant to small angles of inclination. Allen & Perkins (1951) considered large angles of inclination where viscous effects are important. They did this by modelling the cross-flow development by analogy with the flow over an impulsively started cylinder. This has turned out to be a very fruitful approach and has been developed by later workers, for example Sarpkaya (1966) and Bostock (1972).

The out-of-plane force does not exist on bodies of commonly encountered fineness ratios until fairly high angles of inclination and it is only quite recently that it has received much attention. Even now the experimental data available are mostly for overall forces on specific bodies. Examples of such measurements may be found in the work by Atraghji (1967), Pick (1971), Coe, Chambers & Letko (1972), Lamont & Hunt (1973), Wardlaw (1974) and Jorgensen & Nelson (1975). Thomson & Morrison (1971) have contributed important information on the flow field by studying the vortex pattern which exists under these conditions and Thomson (1972) has employed their results in two prediction methods which give upper and lower bounds on the overall out-of-plane force. The only relevant surface pressure measurements are those of Bostock (1972). His main interest was in the in-plane normal force but he also presents out-of-plane force distributions at inclination angles of 15° and 30°.

The present state of knowledge of out-of-plane forces is very unsatisfactory. Apart from Bostock's two results at small angles, no experimental force distributions along the axis have been obtained. Further, the experimental measurements of the overall force show alarming differences between the results of different workers and strong and unpredictable variations with roll angle. There is an urgent need for studies which are more detailed than those which have been reported so far. This paper attempts to meet some of this need as far as flows with laminar boundary layers are concerned. It reports an experimental investigation of surface pressures on a cylindrical body of circular cross-section fitted with various nose shapes for angles of inclination up to 90°. The main concern is with the distribution of out-of-plane force along the body although some in-plane normal force distributions are also presented. The results are interpreted from the viewpoint of the impulsively started cross-flow analogy; this analogy is therefore briefly discussed in the next section. The flow was found to be rather unsteady in a manner which casts certain doubts on the time-averaged results. Some time-dependent measurements were therefore taken to resolve the uncertainties. It was felt that the presentation would be clearest if it was basically chronological and explained the reasons for some of the tests. The apparatus for the time-averaged tests is therefore described in §3 and the results obtained with it are presented together with some preliminary discussion in §4. Following this, the time-dependent tests are described, the results pre-

sented and the reason for the unsteadiness examined. A more complete view is then given in §6 of the reliability of the results and of their interpretation. Finally, examples are given of circumferential pressure distributions at various points along the cylinder and a comparison made with pressure distributions from particular points in a Kármán vortex-shedding cycle.

2. The impulsively started cross-flow analogy

According to the analogy originally suggested by Allen & Perkins (1951), the flow over an inclined cylinder develops from the nose as a result of a sheet of fluid in the cross-flow plane being convected over the cylinder by the axial component of velocity. The cross-flow sheet of fluid is considered to experience the cylinder as though it were impulsively started. The flow development with distance on the inclined cylinder can therefore be related to the flow development with time on the impulsively started cylinder as follows. The non-dimensional time parameter for the impulsively started cylinder is Vt/R, denoted here by $\bar{t}$, where V is the flow velocity and R the radius of the cylinder. On a cylinder at an angle α to a stream of velocity U, V becomes the cross-flow velocity $U \sin \alpha$ and the time for flow development is $x/(U \cos \alpha)$, where x is the distance from the nose. We therefore find that $\bar{t} = (x/R) \tan \alpha$.

Since the flow development on an impulsively started cylinder consists, after an initially symmetric flow, of the growth of a sequence of alternating vortices, the impulsively started analogy explains immediately how an out-of-plane force can arise on a symmetrical body.

In an earlier paper (Lamont & Hunt 1973) we used the impulsively started analogy as the basis of a simple method of estimating the overall out-of-plane force and associated moment on a circular cylinder and compared the predicted values with experimental measurements. The quantitative content of our approximate method used what little information was available but could not be said to be very solidly based. Nonetheless, the results reproduced the complex variations of the experimental values well, and even though there were substantial discrepancies in the magnitudes of the forces, the comparisons supported the impulsively started cross-flow model as a basis for understanding out-of-plane forces. It did not seem to us, however, that a straightforward form of the analogy could be taken any further since adjustments to the more arbitrary values which occurred in our method did not produce a significant improvement in quantitative agreement. It therefore seemed more promising to study the inclined cylinder directly than to attempt to obtain improved impulsively started data.†

Our early approximate method calculated the overall forces from an assumed variation of the out-of-plane force coefficient C_{of} with $\bar{t}$. This distribution is shown in figure 1 and will be compared with the experimentally determined distributions presented later. The force coefficient is based on the cross-flow dynamic head and the cylinder diameter. The distribution was constructed from

† Our ideas on this point were undoubtedly influenced by a discussion with Professor W. A. Mair and Dr B. R. Bostock.

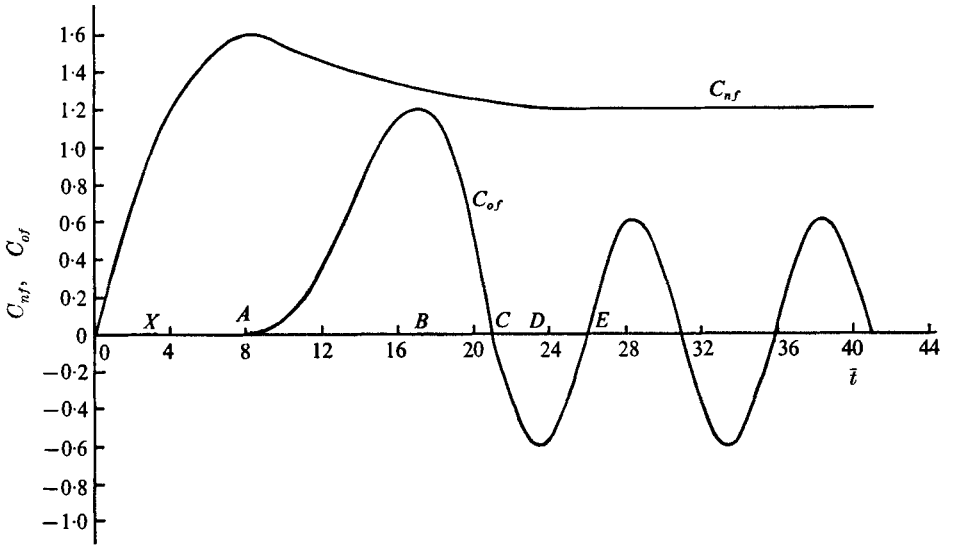

FIGURE 1. Force coefficients on an impulsively started cylinder.

such impulsively started flow information as is available: the vortex shedding points and the point of initial asymmetry were found experimentally by Sarpkaya (1966) but other information is scanty and unreliable. The impulsively started cross-flow prediction of the in-plane normal force distribution C_{nf} is shown on the same figure: it will also be referred to later.

3. Experimental system

The tests were carried out in the University of Bristol's 2·1 m by 1·5 m low-speed wind tunnel. The model used was of circular cross-section, consisting of interchangeable noses on a constant-diameter pressure-tapped body. The main set of tests was concerned with the measurement of the time-averaged pressures and the calculation of corresponding time-averaged forces; the experimental equipment used for these tests is described in this section. It became clear while carrying out the time-averaged measurements that it would subsequently be necessary to measure instantaneous pressures. The equipment used to conduct these time-varying tests is described in §5.1.

3.1. *Pressure-tapped body*

The scale of the body was principally determined by the need to maintain laminar flow down to an acceptable minimum angle of inclination. The work of Bursnal & Loftin (1951) on yawed cylinders shows that, if the characteristic length used to define the Reynolds number is taken as $2R/\sin\alpha$, then the critical Reynolds number for transition to turbulent flow is approximately independent of inclination. Thus the critical Reynolds number can be determined from tests conducted at 90° inclination. Such tests in the tunnel used in this work gave a value of the critical Reynolds number of approximately 2×10^5. In order to

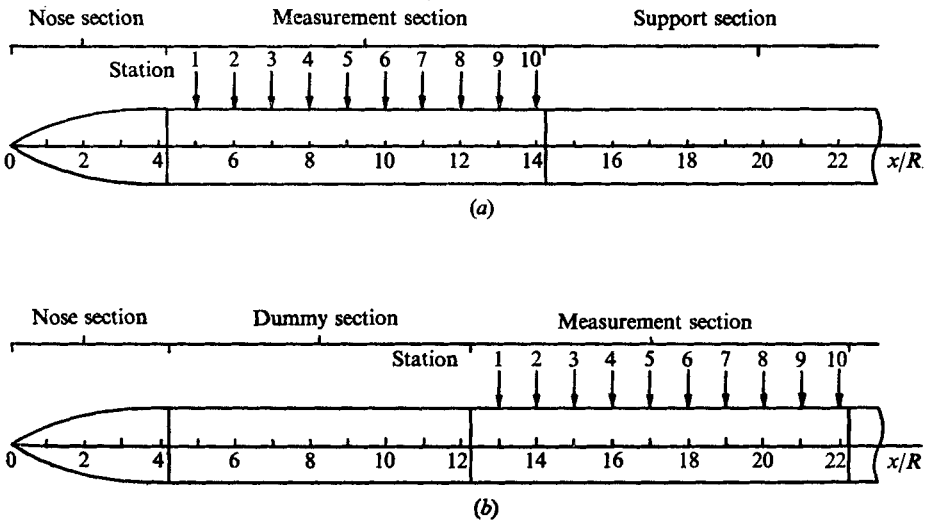

FIGURE 2. Diagram of the model. (*a*) Measurement section in forward position. (*b*) Measurement section in rearward position.

ensure that the boundary layer would remain laminar at separation and not reattach, it was desired to work at Reynolds numbers significantly below the critical value. This requirement, together with the need to maintain the cross-flow velocity above about 8 m s $^{-1}$ in order to achieve reliable pressure measurements, fixed the model diameter at 51 mm. At the main Reynolds number used in these tests of $1{\cdot}1 \times 10^5$ (based on $2R$ cosec α), adequacy of pressure measurement could be achieved with this model down to an inclination angle of 30°.

The extent and resolution of the pressure tappings on the model were chosen with reference to the approximate force distribution shown in figure 1. An axial coverage of nine diameters was chosen in order to cover at least the first half-cycle of the out-of-plane force distribution for inclination angles down to about 30°. At higher inclinations, more cycles could be covered but the rapidity of the axial variation increases and greater resolution was required. An axial spacing of half a diameter was chosen to give adequate definition up to about 70°. A minimum angular spacing of 10° was required. This or better could be achieved by rotating the model. However, this was not considered advisable in view of the work by Atraghji (1967) and by Lamont & Hunt (1973), which showed that the measured value of the out-of-plane force can depend on the roll setting of the model about its axis; if such a variation with roll angle were to occur while rotating the model to collect pressure data, the results would not be self-consistent. A complete angular distribution of pressure tappings with 10° spacing was therefore used at each station. It was not possible to fit all the pressure tubing from 19 stations each with 36 holes within the model without adopting a tubing diameter which was too small for a reasonable response time. Instead, a measuring section containing ten stations (covering $4\frac{1}{2}$ diameters) was used and a separate test conducted on each of two configurations. In one test, the measuring section was mounted directly behind the nose, while in the second

test a dummy section was included between the nose and the measuring section. The arrangement is shown in figure 2. The dummy section was four diameters in length, hence producing an overlap of two stations between the two tests. The problem of fitting the pressure tubing to the tappings was overcome by constructing the measuring section of five subsections which could be screwed together. Each subsection contained two stations, which were therefore easily accessible before assembly.

Four nose shapes were used in the main series of tests. Three were circular-arc ogives whose lengths were 2, 4 and 6 times the cross-sectional radius of the model. The fourth nose was a cone of length 4 times the radius. A limited number of tests were conducted using a $5R$ ogive nose: only brief mention is made of these in the paper.

The cylindrical model was completed by the addition of a constant-diameter support section 0·965 m in length. The support section was firmly clamped in a vertical pylon running between the tunnel walls. The pylon allowed the model to be set at any angular inclination within a horizontal plane. The pylon was 51 mm in diameter and situated some six diameters aft of the most rearward measuring station.

The 360 pressure tubes were passed rearward inside the support section and out of the tunnel through a flexible shield to the pressure recording equipment.

3.2. *Data recording and reduction*

Outside the tunnel the 36 pressure tubes from each of the ten stations were connected to separate Scanivalve connector rings. During a test, each connector ring was fitted in turn to a Scanivalve; in this way, the difference between the pressure at each tapping and the tunnel static pressure was measured by a variable-inductance transducer which had a maximum range of $\pm 0{\cdot}01$ bar. The analog signal from the transducer was amplified and filtered by a low-pass filter which gave a time average of the signal. The output of the filter was then sampled, digitized and recorded on paper tape. The tunnel dynamic pressure was recorded through the same system.

The data were processed in two stages. First, pressure coefficients based on the cross-flow dynamic pressure were calculated and plotted against the angular distribution for each station. These plots were then inspected for erroneous values due to leaks or blockages. (The number of incorrect values was generally only about 2 or 3 out of the 360 readings taken in a test.) Estimates were made of the correct values at such points and the corrected set of pressure coefficients was then used to calculate local force coefficients.

4. The time-averaged results

This section presents and describes the distributions of out-of-plane force which were obtained using the extensively pressure-tapped model described in the previous section. Some discussion of these distributions is included here. However, significant unsteadiness was experienced in the flow, which necessitated a study of the fluctuations in the pressures. This study is reported in §5

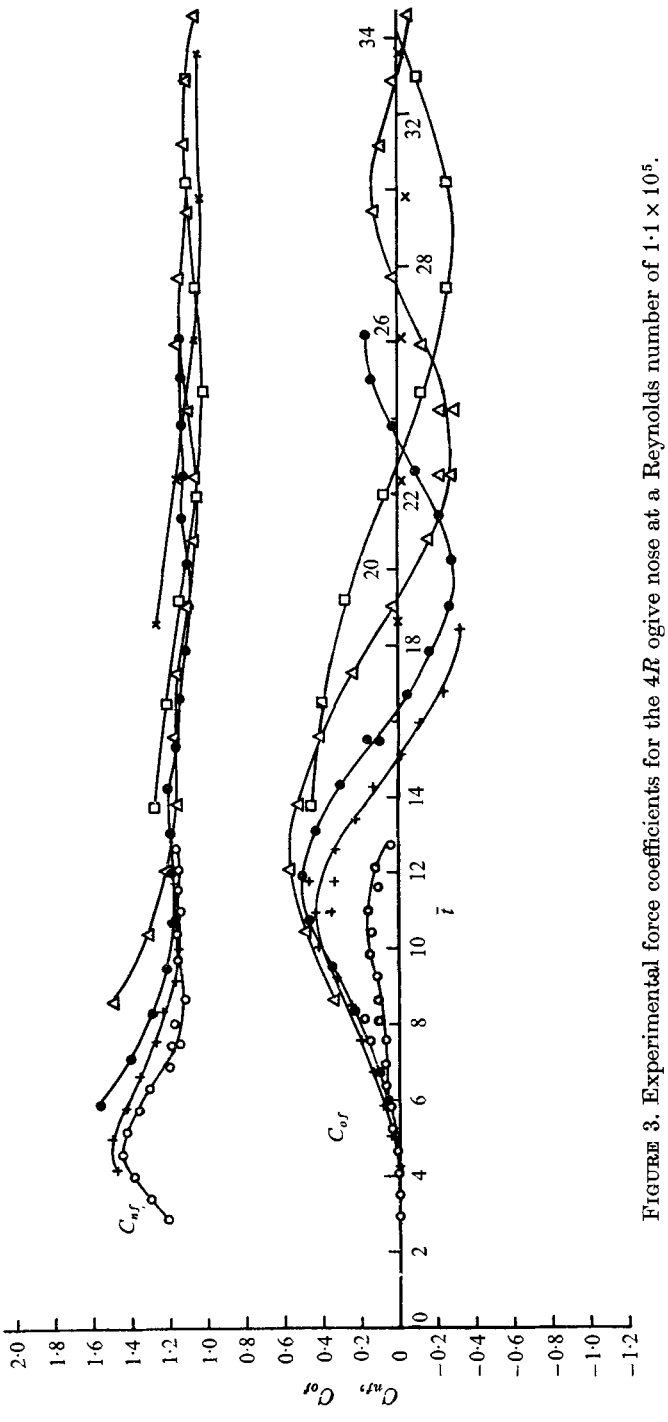

FIGURE 3. Experimental force coefficients for the $4R$ ogive nose at a Reynolds number of $1{\cdot}1 \times 10^5$.

and a discussion taking account of both sets of results is given in §6. The definition of the Reynolds number used throughout the paper is $U(2R \text{ cosec } \alpha)/\nu$, where U is the free-stream velocity and $2R$ cosec α the characteristic length. All the force and pressure coefficients which are presented are based on the cross-flow dynamic pressure.

4.1. *The 4R ogive nose*

In the set of tests described here, the Reynolds number (defined above) was maintained constant at $1{\cdot}1 \times 10^5$. The inclination range 30–75° was covered; two tests were carried out at each inclination, one with and one without the dummy section. In order to confirm that the boundary layer remained laminar up to separation and did not reattach, the pressure distributions were inspected: there was no evidence of reattachment at the Reynolds numbers of the tests reported here. Exploratory tests at higher Reynolds numbers were conducted; at a value of 2×10^5, the pressure distributions still indicated the existence of laminar separation without reattachment but the influence of turbulent reattachment could be seen in the results of a test carried out at a value of $3{\cdot}0 \times 10^5$. Several examples of experimental pressure distributions may be found in figures 23–26 (which will be discussed in more detail in §7). In particular, figure 26 contains three examples of pressure distributions obtained for a Reynolds number of $1{\cdot}1 \times 10^5$ at points where the flow is symmetric. It can be seen that these distributions are similar to those found on a 'two-dimensional' cylinder under conditions of laminar separation. Figure 3 shows values of the local out-of-plane force coefficient C_{of} and of the local in-plane normal force coefficient C_{nf} plotted against the equivalent impulsively started time parameter $\bar{t} = x \tan \alpha/R$. Both coefficients are made non-dimensional by means of the cross-flow dynamic head and the cylinder diameter. In most cases throughout the entire experimental programme, the first half-cycles of the out-of-plan force distributions were in the same sense. When results of opposite sense were recorded, they were reversed for clarity. The two stations where an overlap occurs can be identified on each curve of figure 3; it can be seen that the values are in reasonable but not exact agreement. Results were also obtained at intermediate values of the inclination angle, α, but are omitted from the figure for clarity.

According to the impulsively started analogy, all the results for each coefficient should fall on a single curve as on figure 1, the in-plane normal force should show a maximum value at the onset of asymmetry and then fall to a constant value while the out-of-plane force should vary periodically with $\bar{t}$. The curves in figure 3 do show these variations but they also depend on the angle of inclination.

The in-plane force C_{nf} rises to a maximum value which is in the neighbourhood of the impulsively started value of 1·6. It then falls to a constant value, which is approximately 1·0, compared with the value of 1·2 found in impulsively started flow. Some oscillation of C_{nf} appears to be present, the period increasing with the value of α.

The out-of-plane force coefficient C_{of} shows a much more marked periodicity

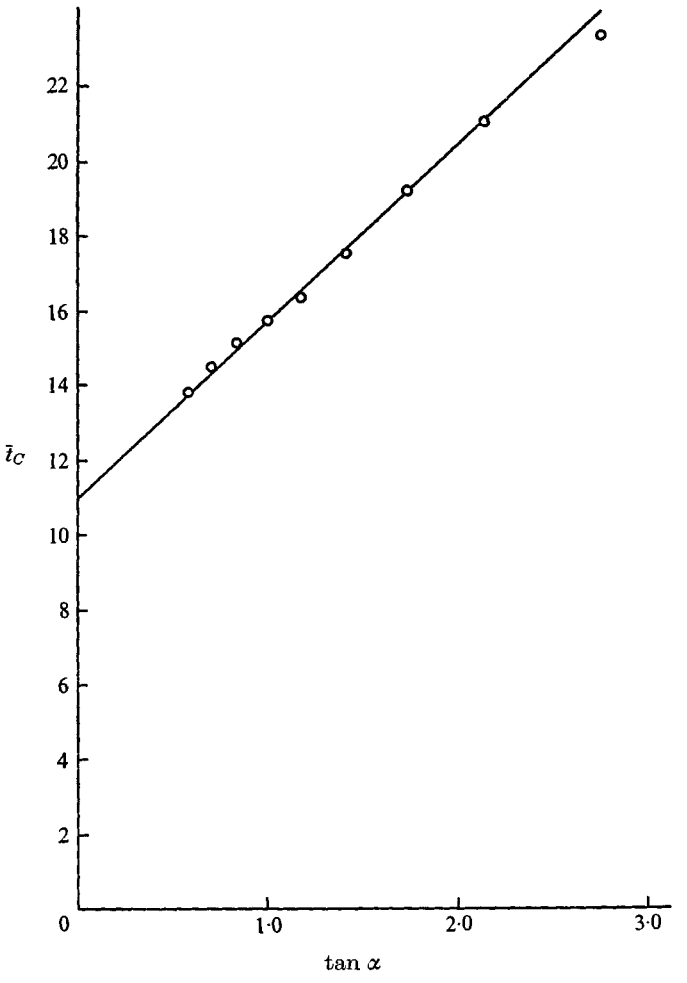

FIGURE 4. Variation of first node point with angle of inclination for the $4R$ ogive nose at a Reynolds number of $1{\cdot}1 \times 10^5$. ——. $\bar{t}_C = 11 + 4{\cdot}7 \tan \alpha$.

although only for about three half-cycles, suggesting that only three vortices are shed. Further, the spacing between node points (i.e. the distances equivalent to AC and CE on figure 1) increases with α; on the other hand, the onset of asymmetry does not vary detectably from the point $\bar{t} = 5$ (compared with $\bar{t} = 8$ in the simple form of the analogy). The value $\bar{t}_C$ of $\bar{t}$ at the first node point C was obtained from figure 3 and plotted against $\tan \alpha$ in figure 4. The values are found to lie remarkably well on a straight line with intercept 11 and slope 4·7.

The amplitudes of the out-of-plane force variations also show a variation from one curve to another although not in a completely consistent manner. The peak value of C_{of} at the shedding of the first vortex is in the range 0·4–0·6 for $\alpha \leqslant 70°$, except at $\alpha = 30°$ and 35°, where the values are only about 0·2. An examination of some of the instantaneously sampled values at these two lowest inclinations indicated that the flow was very unsteady, so that, although the values

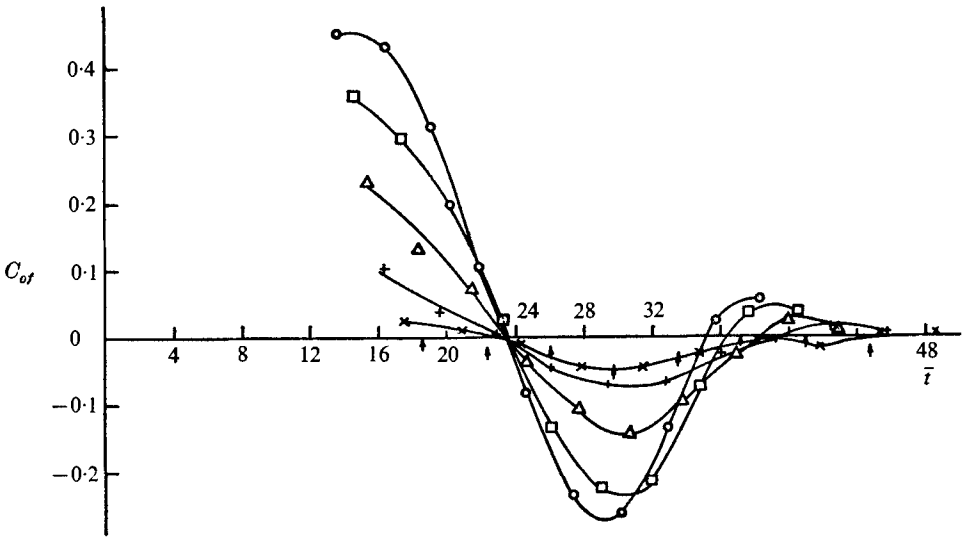

FIGURE 5. Reduction of out-of-plane force at high angles of inclination for the $4R$ ogive nose at a Reynolds number of $1{\cdot}1 \times 10^5$.

	○	□	△	+	×	↑
α (deg)	70	71	72	73	74	75

plotted may be true time-averaged quantities, they are unlikely to be equal to the maximum instantaneous values. Flow unsteadiness in one form or another made the interpretation of all the time-averaged results considerably more difficult and a number of points (including this question of the maximum value of the force coefficient) could not be finally resolved without the time-varying measurements described in §5.

A number of tests were performed to check on the repeatability of the experimental results. Some variation in the peak values of C_{of} was found but the repeatability of the positions of the node points on the distributions was very good. The rapid disappearance of the out-of-plane force between inclinations of 70° and 75° was confirmed. This behaviour was investigated in more detail by a series of tests carried out at 1° intervals from 70° to 75°. The results are presented in figure 5 and show a progressive reduction to zero of the out-of-plane force.

4.2. *Other nose shapes*

The effect of nose shape was investigated in a series of tests at a Reynolds number of $1{\cdot}1 \times 10^5$. Ogive noses of lengths $6R$ and $2R$ and a $4R$ conical nose were used.

Figure 6 shows the results obtained for the $6R$ nose. A number of differences can be seen from the curves for the $4R$ nose plotted in figure 3. The most striking difference is in the magnitudes of the out-of-plane force. The peak value of C_{of} is now about 1·5, compared with 0·6 for the $4R$ nose. As far as the spacing is concerned, the onset of asymmetry appears to occur slightly earlier than on the $4R$ nose: the value of $\bar{t}$ at this point is approximately 4, compared with 5 for the

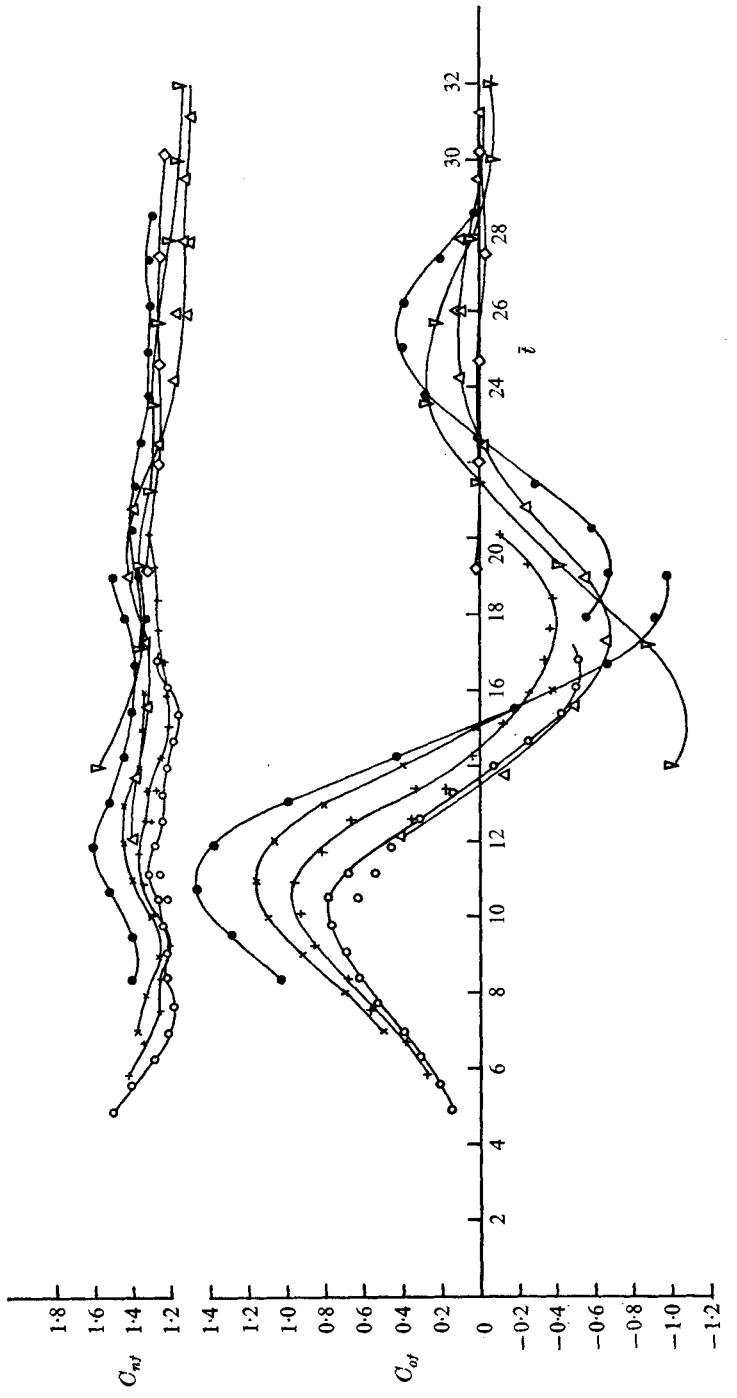

FIGURE 6. Experimental force coefficients for the 6*R* ogive nose at a Reynolds number of $1{\cdot}1 \times 10^5$.

$4R$ nose. Also, the movement of the first node point $\bar{t}_C$ follows the straight line of figure 4 for values of α up to 50°, thereafter appearing to fall slightly. It should be pointed out that the result for $\alpha = 65°$ is difficult to interpret since so much of the flow development occurs on the nose. In particular, it is not clear whether the peak in C_{of} at $\bar{t} = 15$ is due to the shedding of the second vortex or to the shedding of a first vortex with opposite sense to those normally encountered. The larger values of C_{of} seen on figure 6 are accompanied by increased values of the normal force coefficient C_{nf}.

Some additional tests, involving only some stations, were performed with the $6R$ nose at values of α of 30°, 55° and 67·5°. These suggest that the greatest value of $\hat{C}_{of1}$, which denotes the first peak value on the distribution of C_{of} for a fixed inclination, is 1·7 and occurs at an inclination of 55°. They also show that the out-of-plane force has virtually disappeared at an inclination of 67·5° (compared with a value of 75° with the $4R$ ogive nose).

The results for the $2R$ ogive nose are presented in figure 7. The distributions of C_{of} are similar to those obtained for the $4R$ ogive nose. Thus the maximum value obtained for $\hat{C}_{of1}$ is again 0·6, the out-of-plane force drops to virtually zero by an inclination of 74°, the onset of asymmetry is approximately at the point $\bar{t} = 5$ and the point $\bar{t}_C$ follows the straight line of figure 4. A difference is that the position of the maximum normal force coefficient varies quite markedly with the angle of inclination.

Finally, the results for the $4R$ conical nose are presented in figure 8. They are similar to those obtained for the $6R$ ogive nose, presented in figure 6. The out-of-plane force coefficients are large: the maximum recorded value is over two and even the second shedding point produces magnitudes up to 1·2. The out-of-plane force disappears between inclinations of 60° and 70°. Asymmetry occurs early, at a value of $\bar{t}$ of about 3. The lowest inclination at which $\bar{t}_C$ can be determined from these results is 45°. The value is then 14, which puts it slightly below the straight line of figure 4. Above 45° inclination, $\bar{t}_C$ falls with increasing angle. The normal force coefficient is generally larger than those found on the ogive noses.

4.3. *Discussion of the influence of the nose on* C_{of}

Although the reliability of the results presented so far is open to doubt because of the unsteadiness observed, nonetheless the striking effect of nose shape on the values of C_{of} will be shown later to be significant and is given a preliminary consideration here.

In the tests reported so far, much larger out-of-plane forces were experienced on the $6R$ ogive and $4R$ cone noses than on the $4R$ and $2R$ ogive noses. Now, the main difference in the flows over these noses is that much more asymmetric flow occurs on the $6R$ ogive and $4R$ cone noses than on the $4R$ and $2R$ ogive noses. In the case of the $4R$ cone, this is due to the early onset of asymmetry while on the $6R$ nose a slightly earlier occurrence of asymmetry is coupled with the greater nose length. A more detailed study of figures 6 and 8 suggests that the peak coefficient $\hat{C}_{of1}$ on the afterbody increases as the proportion of asymmetric flow development on the nose increases, up to a maximum which

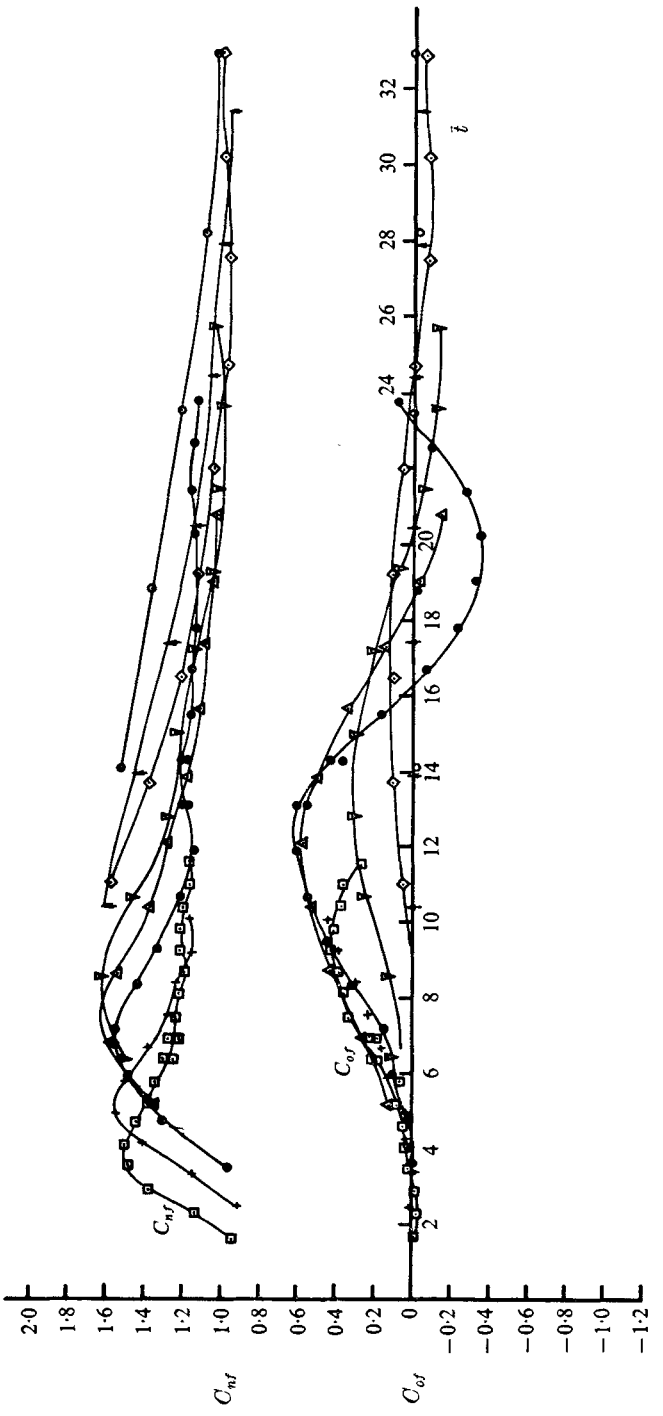

FIGURE 7. Experimental force coefficients for the $2R$ ogive nose at a Reynolds number of $1{\cdot}1 \times 10^5$.

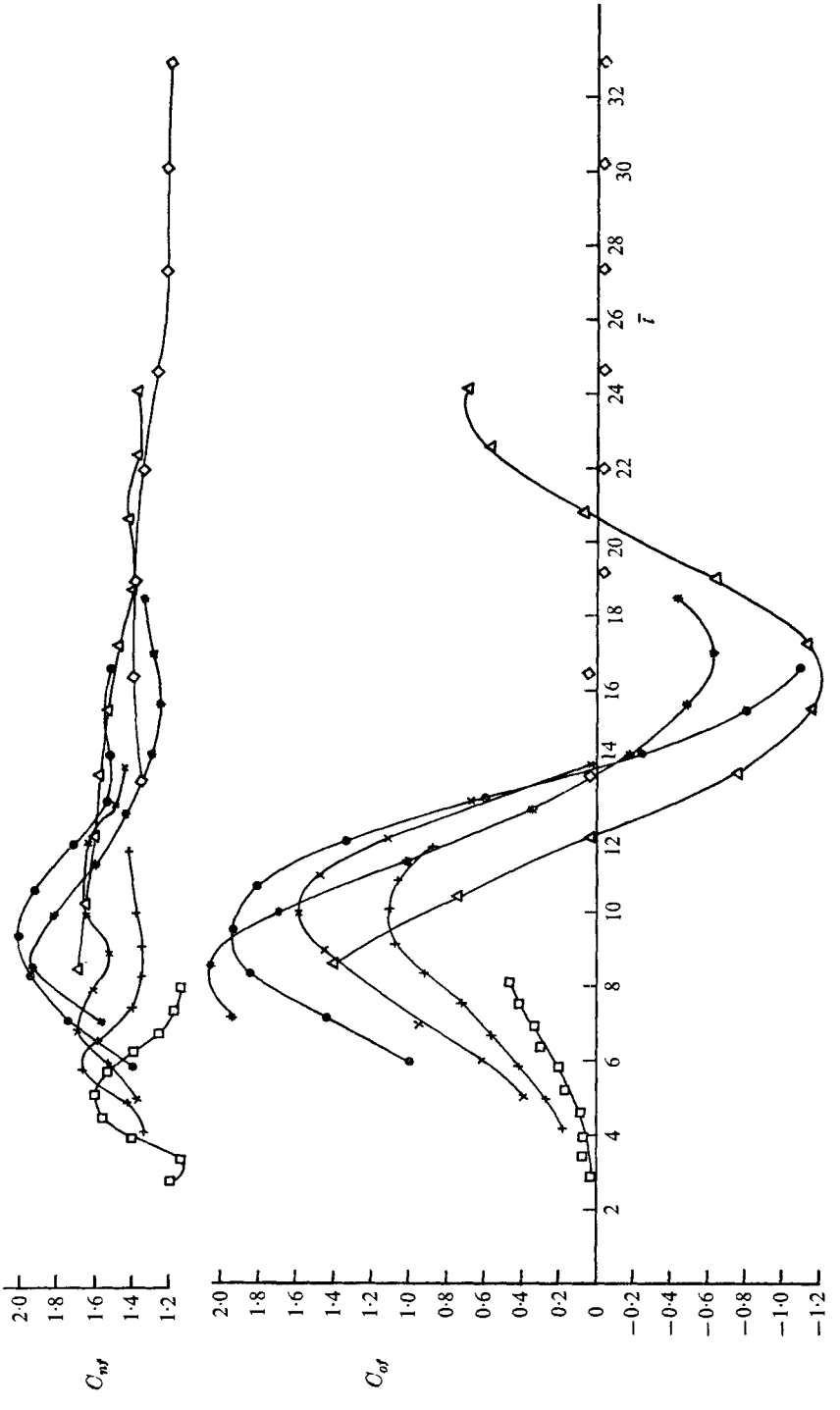

FIGURE 8. Experimental force coefficients for the $4R$ cone nose at a Reynolds number of $1{\cdot}1 \times 10^5$.

corresponds to the occurrence of the peak force (and hence, presumably, the first vortex shedding) in the vicinity of the junction of the nose with the afterbody. It thus seems that larger asymmetries are produced when the vortex growth takes place in the pressure field of the expanding nose region than are produced when the growth occurs along the constant-area body. It may also be that the differences which have been noted in the point of onset of asymmetry are due to a similar effect.

Now above 51° inclination, asymmetric flow occurs on the $4R$ ogive nose and the hypothesis just presented implies that increased values of $\hat{C}_{of1}$ should then occur with a maximum at about 65°. Some confirmation of this is provided by the earlier overall force tests reported by Lamont & Hunt (1973) and summarized in §2. These tests used a model with a $4R$ ogive nose which produced a maximum overall force at an inclination of about 65°. Furthermore, the recorded maximum value would require the first vortex to give a peak value of C_{of} of about 1·8. Yet no value greater than 0·65 was recorded in the tests reported in this section. An attempt was therefore made to find larger values of $\hat{C}_{of1}$ by varying the roll angle and Reynolds number. These studies are reported in the next two subsections.

4.4. *Effect of varying roll angle*

Roll-angle tests were first conducted with the $4R$ nose at 50° inclination and at the main test Reynolds number of $1{\cdot}1 \times 10^5$. The roll angle was varied in steps of 30° from 0 to 180°, the datum being the roll angle used in all the preceding tests. The resulting force coefficients are presented in figure 9. It can be seen that the values of C_{nf} are only slightly affected by the roll angle but that C_{of} is greatly influenced, the peak values varying from 0·23 to 0·81. The tests in which the lower values were recorded showed evidence of unsteadiness.

Although the magnitude of C_{of} is influenced by the roll angle, it is important to note that the shape of the curves is not. In particular, the positions of the peak and of the node point $\bar{l}_C$ are virtually independent of the roll angle. Because of this, it is possible to investigate the influence of the roll angle on $\hat{C}_{of1}$ by studying only one or two carefully selected stations. Taking advantage of this possibility, further tests were conducted at various roll angles at inclinations of 60° and 65°. The results for 65° are presented in figure 10. The maximum value recorded was again only 0·8. On the basis of this evidence, then, it seems unlikely that time-averaged coefficients as high as 1·8 can be obtained under these conditions by varying the roll angle alone.

4.5. *Effect of varying Reynolds number*

Tests on the model with the $4R$ ogive nose in the range of inclination angles 60–65° were conducted for Reynolds numbers between 4×10^4 and $1{\cdot}1 \times 10^5$. The results at 60° inclination are shown on figure 11 (*a*). It can be seen that there is a distinct and consistent increase in the peak out-of-plane force coefficient $\hat{C}_{of1}$ as the Reynolds number is reduced. There is also a simultaneous movement of the node point C towards the nose. The single point obtained for a Reynolds number of 4×10^4 suggests that a modest further reduction below this value

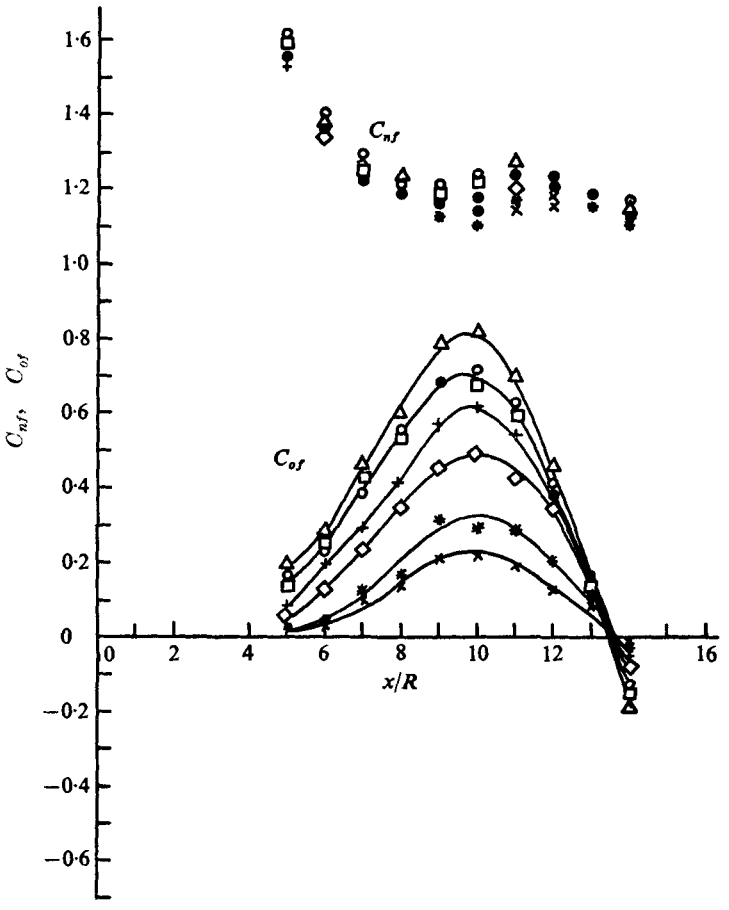

FIGURE 9. Force coefficients at various roll angles for the $4R$ ogive nose; $\alpha = 50°$, $Re = 1{\cdot}1 \times 10^5$.

	○	×	□	△	*	◇	+	●
ϕ (deg)	0	30	60	90	120	150	180	Coincident points

will not produce any further increase in $\hat{C}_{of1}$. However, it was not possible to check this since the accuracy of the experiments was not sufficient at such low velocities. For a Reynolds number of $1{\cdot}5 \times 10^5$, the value of $\hat{C}_{of1}$ was 0·51 and the point C coincided with its position at a Reynolds number of $1{\cdot}1 \times 10^5$, suggesting that no further change occurs until the influence of turbulent reattachment is felt. Similar behaviour was observed in tests involving the $5R$ and $6R$ ogive noses.

A number of tests were conducted on all the ogive noses at lower inclinations. The positions of the point C and the values of $\hat{C}_{of1}$ were found to be independent of Reynolds number over the range $4 \times 10^4 < Re < 1{\cdot}5 \times 10^5$ for angles of inclination below 60°.

At inclinations of 60° and above, where the variation with Reynolds number was observed, a substantial amount of the development of the first vortex

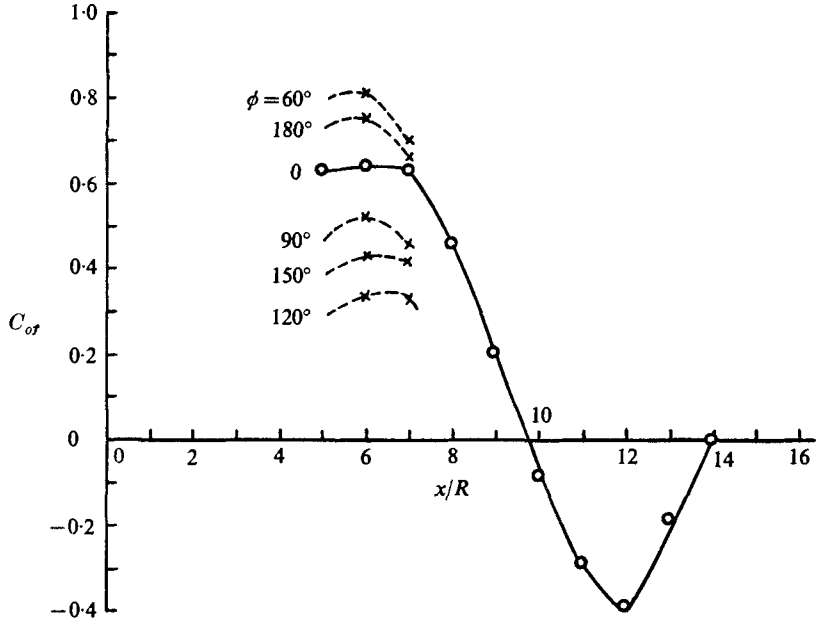

FIGURE 10. Out-of-plane force coefficient at various roll angles for the $4R$ ogive nose; $\alpha = 65°$, $Re = 1{\cdot}1 \times 10^5$.

occurs on the nose for the $4R$, $5R$ and $6R$ ogives. For the $2R$ nose, however, relatively little asymmetry occurs on the nose at 60°. Figure 11(*b*) shows that, even so, a substantial Reynolds number dependence exists. It seems, therefore, that this Reynolds number effect is not associated with the development of asymmetric flow over the nose; more probably, it is due to the close spacing of the vortices and high axial gradients which arise at high angles of inclination.

4.6. *The influence of unsteadiness on the time-averaged results*

The evidence obtained from the time-averaged results has shown that unsteadiness exists in the flow which influences the time-averaged measurements, particularly the measurements of the out-of-plane force. The results of the roll-angle tests and of a considerable number of checks on repeatability show that the spacings of the distributions are little affected by different levels of unsteadiness although the magnitudes of the force can be strongly affected. It is also noteworthy that there is relatively little sign of scatter between different stations on the body in any one test. These observations suggest that the unsteadiness takes the form of wholesale switching of the flow pattern between its two possible configurations, of which one is preferred. (The time-dependent tests described in the next section show that this is a substantially correct although over-simplified view.)

Of the variations in the amplitude of the out-of-plane force distributions which were discovered in the time-averaged tests, the evidence suggests that the following are due to flow switching: (i) the lack of complete repeatability, (ii) the discrepancies between values measured at the overlap stations in each

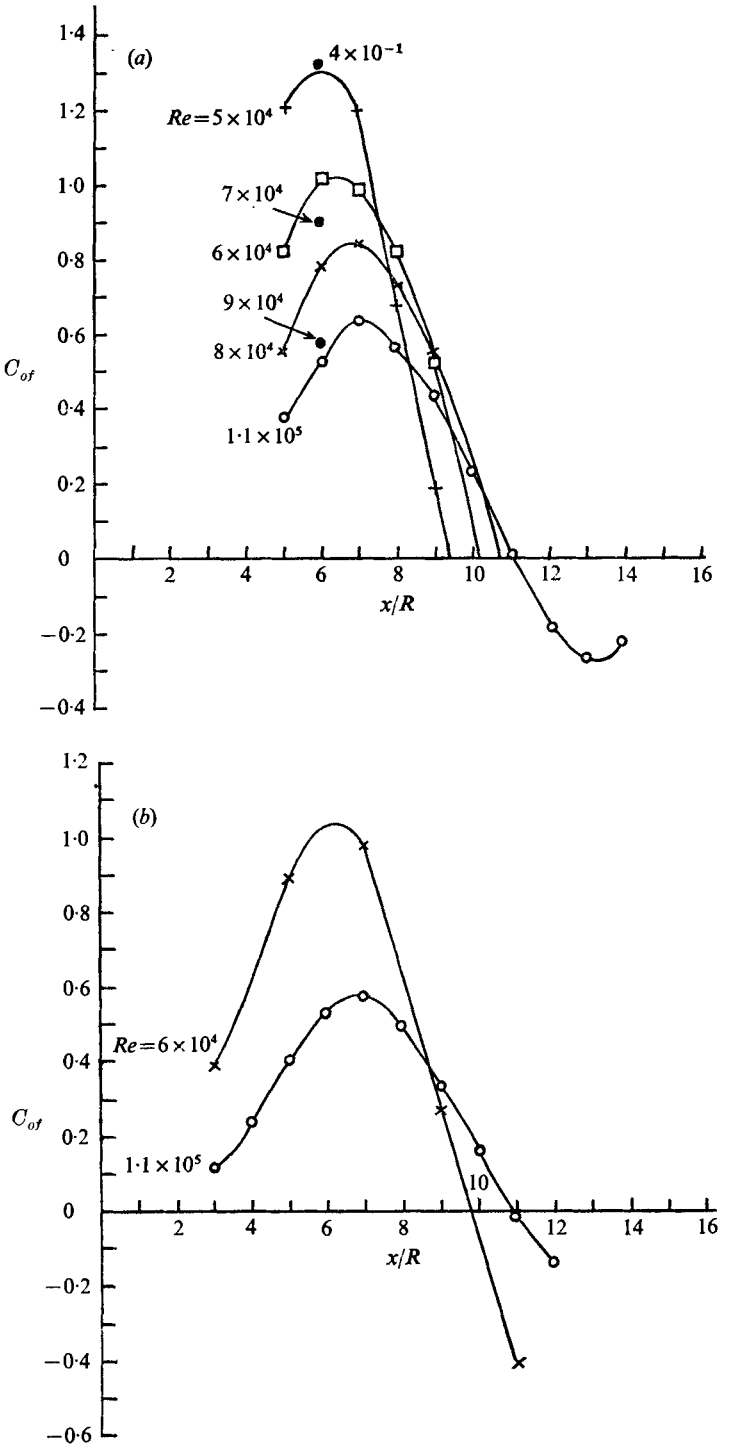

FIGURE 11. Effect of Reynolds number on out-of-plane force for (*a*) the $4R$ and (*b*) the $2R$ ogive nose; $\alpha = 60°$.

pair of tests conducted with and without the dummy section and (iii) the large variations with roll angle. On the other hand, the increase in the out-of-plane force when asymmetry occurs on the nose and the variation with Reynolds number seem to be real effects and not due to flow switching.

The next section describes an investigation into the unsteadiness.

5. The time-dependent measurements

5.1. *Experimental method*

In order to conduct a complete study of the fluctuating nature of the flow, it would be necessary to monitor the pressures at a number of points around the cylinder by means of a multiple-channel measuring system. This technique has been used by Gerrard (1961) and Drescher (1956) to study the fluctuating lift force on a cylinder normal to the stream. Such a method was beyond the resources of time and equipment available in this work.

Instead, a simpler method was employed which could still provide useful information about the behaviour of the flow. This method is based on the notion of flow switching which was outlined in §4.6. Now if the flow switches between two mirror-image states, then the maximum possible steady value of the out-of-plane force at any station is that which occurs in either of the two alternative states and it is this quantity which must be determined if we are to describe the ideal, unswitched flow and force distribution. Suppose, therefore, that we continuously monitor the pressure difference between a hole on the upper surface of the cylinder and the corresponding hole on the lower surface; then it should be possible from the output to identify the maximum magnitude of the pressure difference and the extent of switching. If this is repeated for each pair of holes, the distribution of the pressure difference in the unswitched state can be obtained and the maximum sustainable force evaluated.

This process requires only one channel of equipment. Furthermore, if the variations of pressure with circumferential position and the distributions of force with axial position have the same forms in the time-averaged tests as they do in the unswitched state, then we can reduce the time-dependent measurements to a few pairs of holes at each of a small number of stations. Note that the similarity of distributions of pressure and force which is assumed in this technique will hold if wholesale switching of the flow patterns is occurring.

Following this approach, a new measurement section was constructed containing four stations equivalent to stations 2, 4, 6 and 8 of the original (see figure 2). These stations were chosen since they are in the vicinity of the peak force at the angles of greatest interest. The pressure tappings were located at $\theta = \pm 45°$, $\pm 75°$, $\pm 105°$ and $\pm 135°$. These positions are symmetrical about $\theta = 90°$ and enable tests to be performed at roll angles of both 0 and 180°; they also provide enough points for some comparison to be made between the shapes of the inferred unswitched pressure distributions and the corresponding time-averaged distributions. The pressure transducer was housed within the model and connected to the surface tappings by short (approximately 70 mm)

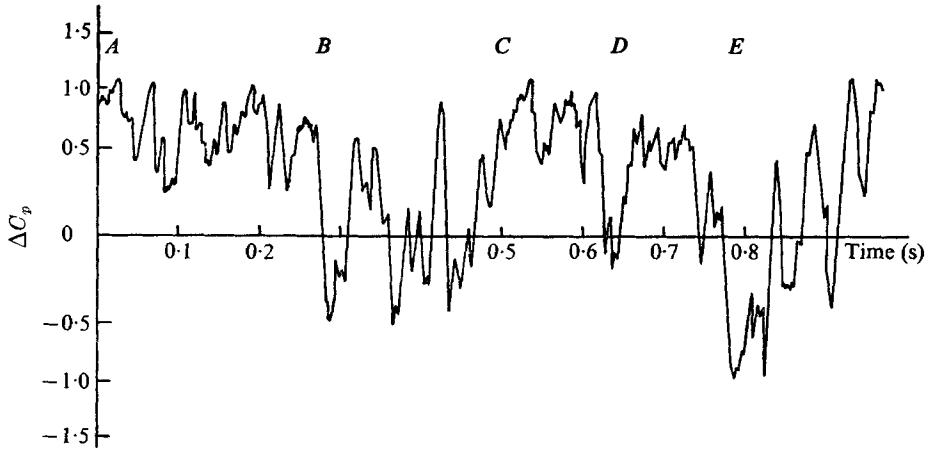

FIGURE 12. Time-dependent behaviour of the pressure difference at $\pm 75°$ from the front of the cylinder at $x/R = 14$ for the $4R$ ogive nose; $\alpha = 30°$, $Re = 1{\cdot}1 \times 10^5$.

lengths of polythene tube. The amplified signal from the transducer was recorded on a U, V recorder.

The experimental system was first tested with the model at 90° inclination at a Reynolds number of $1{\cdot}1 \times 10^5$. At each of the four pressure-differencing positions the U, V traces were sinusoidal and corresponded to a Strouhal number of 0·2. The amplitude of the traces varied in the manner reported by Gerrard (1961) and by Drescher (1956) but corresponded to a range of peak lift coefficients of 0·3–0·6 rather than the range 0·6–1·3 quoted by Drescher. This may have been due to the fact that the experimental body did not span the tunnel.

5.2. *Experimental results*

5.2.1. *The 4R ogive nose at 30°–50° inclination.* Figure 12 shows a typical trace obtained from the station $x/R = 14$ at 30° inclination (note the nonlinear pressure scale). This station is near the point of maximum out-of-plane force coefficient. The trace may be interpreted as follows. Between A and B, a constant general level of pressure difference is maintained but with substantial disturbances occurring. Then between B and C the level becomes very disturbed, changes in sign occurring although no complete switch occurs. From C to E, the general level returns to that maintained between A and B except for a brief disturbance at time D. Finally, at E, the pressure switches to an equal and opposite level before switching back again. Clearly, the time average of these values is less than the average value sustained between A and B but is not zero.

This trace suggests that the flow has a preferred state which produces a particular pressure difference at a particular station on the body. But, at this inclination and in this air stream, the flow pattern and accompanying level of pressure difference are frequently disturbed, occasionally to the extent of switching sign to a mirror-image state. However, the transient behaviour of the pressure difference is not simply a steady level intermittently switching

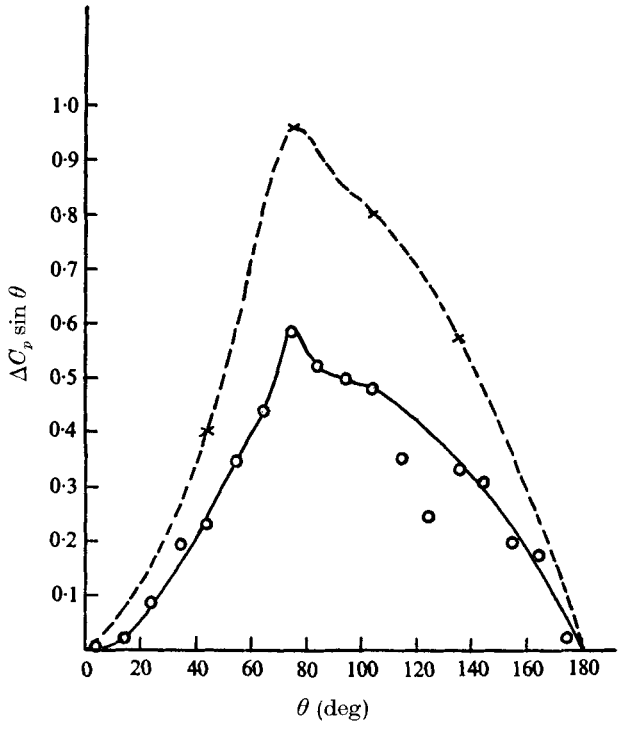

FIGURE 13. Comparison of circumferential pressure distributions at $x/R = 14$ for the $4R$ ogive nose; $\alpha = 30°$, $Re = 1{\cdot}1 \times 10^5$. ×, time-dependent test; ○, time-averaged test.

over to the opposite state as suggested in §4.6. Instead it is further complicated by the frequent occurrence of reductions in the pressure difference to values which lie between the two mirror-image states. A possible explanation for this form of behaviour is offered in §5.3.

A maximum sustainable force coefficient was estimated as follows. A maximum sustainable pressure difference ΔC_p was estimated from each of the traces and a ratio formed with the equivalent time-averaged value. The four ratios were approximately equal. The average value was then used to scale up the peak lift coefficient $\hat{C}_{of1}$ to give a value of the maximum sustainable peak lift coefficient of 0·92, compared with the time-averaged value of 0·55. A similar test conducted at a roll angle of 180° again produced a value of about 0·92 for $\hat{C}_{of1}$. The values of $\Delta C_p \sin\theta$ obtained from the continuous-recording test at zero roll angle and an equivalent time-averaged test are plotted in figure 13. Although the six points (including the zeros) from the continuous-recording tests do not define a curve in detail, it can be seen that they are consistent with the shape of the time-averaged curve.

The traces obtained in tests at 40° and 50° inclination are similar to those at 30° inclination, but there is a decreasing amount of flow disturbance as the angle of inclination increases. The test at 40° inclination indicates a maximum sustainable value of $\hat{C}_{of1}$ of 0·91, which should be compared with the maximum value of $\hat{C}_{of1}$ obtained in the time-averaged tests of 0·70. The figures for 50° inclina-

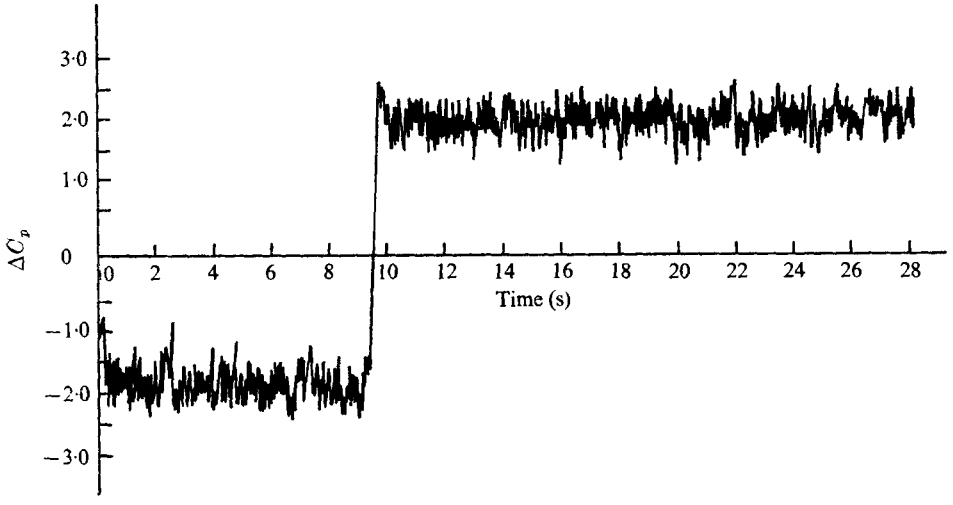

FIGURE 14. Time-dependent behaviour of the pressure difference at 75° from the front of the cylinder at $x/R = 6$ for the $4R$ ogive nose; $\alpha = 60°$, $Re = 6 \times 10^4$.

tion are 1·00 and 0·83 respectively. Tests at roll angles of both 0 and 180° were performed at 50° inclination. As at 30° inclination, both tests produced the same estimate of $\hat{C}_{of1}$. This suggests that the variations with roll angle of the amplitude of the distribution which were discovered during the time-averaged tests (see §4.4) are a result of differences in the amount of flow disturbance occurring at the various roll angles. Both sets of traces are very disturbed at 30° inclination and it is not possible to detect differences between the two roll orientations tested. However, at 50° inclination the traces from one test do appear less disturbed than those obtained at the other roll angle.

5.2.2. *The 4R ogive nose at inclinations of 60° and above.* Tests at these inclinations were performed at Reynolds numbers of $1{\cdot}1 \times 10^5$ and 4×10^4. The traces obtained at 60° inclination and the higher Reynolds number were similar to those obtained at the lower inclinations, but somewhat less disturbed. The inferred maximum sustainable value of $\hat{C}_{of1}$ was 1·04, compared with a value of 0·65 obtained in the time-averaged tests. At 60° inclination the traces for the lower Reynolds number show a much smaller band of variation and provide the first example of a clear switch from one state to the other; this is shown in figure 14. The corresponding estimate of the maximum sustainable value of $\hat{C}_{of1}$ is 1·42, compared with a time-averaged value of 1·32. These tests therefore confirm that the Reynolds number has a substantial influence at this inclination.

At inclinations of 65° and 70°, clean switching from one state to another occurred more often: the dependence of $\hat{C}_{of1}$ on Reynolds number was again confirmed. At 75° inclination, the switching was even more frequent with neither state preferred, so that the time average of the out-of-plane force was zero, as measured in the previous tests. It might be expected that the flow pattern was now of a vortex-shedding type. However, the trace was not sinusoidal and the frequency was much lower than that given by Surry & Surry's (1967) expression for an infinite yawed cylinder. It may be that the flow pattern is

in some sense transitional to conventional vortex shedding since at 80°, although the fluctuations remained rather irregular, it was possible to identify a dominant frequency close to the vortex-shedding frequency. Furthermore, results obtained further aft along the body at higher inclinations were sinusoidal at the vortex-shedding frequency.

Finally, tests were performed with the $4R$ nose at 50° and 60° inclination to find values for the ratio of the magnitude of the second peak in the distribution to the magnitude of the first peak. These ratios were 0·65 and 0·6 respectively.

5.2.3. *6R and 2R noses.* The effect of nose shape was investigated at a Reynolds number of $1{\cdot}1 \times 10^5$ using the $6R$ and the $2R$ noses at inclinations of 30° and 50°. The nature of the disturbances observed was very similar to that seen with the $4R$ nose. The maximum sustainable level of $\hat{C}_{of1}$ at 30° inclination was 1·0 for the $6R$ nose and 0·8 for the $2R$ nose, compared with 0·92 for the $4R$ nose. Corresponding values at 50° inclination were 1·92, 1·0 and 1·04. Thus it appears that, when there is no asymmetry on the nose, the value of $\hat{C}_{of1}$ is approximately 1·0 for all ogive noses, but when asymmetric flow begins on the nose, the value of $\hat{C}_{of1}$ is greatly increased with the value reached depending on the nose shape.

5.3. *An explanation of the transient behaviour*

At large values of $\bar{t}$, the transient behaviour is of a regular, vortex-shedding type. At smaller values of $\bar{t}$, however, the most striking behaviour consists of rapid departures from a preferred state towards and sometimes into a mirror-image state. This irregular behaviour suggests that some form of disturbance is responsible for switching the flow pattern from its preferred state. The most likely source of such disturbances is turbulence in the free stream; turbulent eddies will be convected over the cylinder and the circulation associated with each eddy will influence the local value of the circulation about the body at any instant. In this subsection, this basic notion is developed to give semi-quantitative explanations for the main features of the unsteady behaviour. First, an estimate is made of the frequency of occurrence of eddies which are strong enough to produce significant disturbances to the flow pattern. A similar approach has been used by Tunstall & Harvey (1968) to explain the switching of secondary circulation in the flow around pipe bends.

Suppose, first, that the local value of the out-of-plane force F_{of} is related to the local value of the circulation by the conventional relationship $F_{of} = \rho UK$, where U is the full free-stream velocity and K is the circulation around a path in a plane which is perpendicular to the plane of inclination and which contains the free-stream direction. Then, since C_{of} is based on the cross-flow velocity, we get

$$K = \sin^2 \alpha URC_{of}. \tag{1}$$

Now the mean-square circulation around a circular path in a field of isotropic turbulence is given by Townsend (1956, p. 121) as

$$K_m^2 = 4\pi R_c L_u \overline{u^2}, \tag{2}$$

where L_u is the scale of the turbulence in the stream direction, $\overline{u^2}$ is the mean-square component of the tubulent velocity in the stream direction and R_c is the

radius of the circular path. We choose $R_c = R/\sin\alpha$, so as to enclose the body. L_u and $\overline{u^2}$ can be measured and, hence, although the turbulence will not be perfectly isotropic we can obtain a reasonable estimate of the root-mean-square circulation of eddies of the required scale by taking the square root of (2). This can now be compared with (1). Suppose that a turbulent eddy with circulation equal to one half the local value given by (1) is required to produce a significant disturbance. Denote this value by K_D; then we have from (1) and (2)

$$\frac{K_D}{K_m} = \frac{1}{4}\frac{\sin^3\alpha\, C_{of}}{\pi(L_u \sin\alpha/\pi R)^{\frac{1}{2}}\,(\overline{u^2})^{\frac{1}{2}}/U}. \tag{3}$$

Turbulence measurements were made in the undisturbed flow in the wind tunnel at velocities equivalent to a Reynolds number of $1{\cdot}1 \times 10^5$ at inclinations of 30° and 50°. At 30°, (3) gives $K_D/K_m = 2{\cdot}53C_{of}$. Thus, at the station where the trace in figure 12 was obtained, we get $K_D/K_m = 1{\cdot}9$. Assuming a Gaussian distribution and remembering that only eddies of opposite sense to that of the established circulation will produce a switch, we get a probability P of occurrence of eddies of this strength or greater of 0·0287. The frequency of occurrence is given by $n = PU \sin\alpha/2R$, which gives a frequency of occurrence of serious disturbances of about $4{\cdot}7\ \mathrm{s}^{-1}$.

This figure is distinctly lower than that to be seen on the experimental trace on figure 12. However, the reason for this is that the flow pattern at any station will be influenced by events nearer the nose, where the flow is developing. In particular, the flow will be particularly sensitive to disturbances in the region where the asymmetry between the two vortices has just begun to develop. Such disturbances will be more frequent as well as more effective since the circulation about the body is small. For example, if we consider a point near the start of asymmetry where $C_{of} = 0{\cdot}1$, the frequency of substantial disturbances is $25{\cdot}3\ \mathrm{s}^{-1}$. If we suppose that these disturbances are transmitted aft along the body then they, together with the locally occurring disturbances, will give an overall frequency of disturbances of about $30\ \mathrm{s}^{-1}$, which is approximately correct. (Note, however, that the precise strength of circulation chosen to represent the region of developing asymmetry was arbitrary.) Furthermore, the eddy transport time is $6{\cdot}2 \times 10^{-3}$ s, which is of the order of the duration of the major disturbances of figure 12.

So far we have only considered the influence of disturbances which are opposed to the vortices bound to the body. However, if the behaviour described above is generally correct, it is clear that, whereas an opposing eddy passing over the sensitive, developing region is capable of producing a switch towards the mirror-image state, an eddy having the same sense as the predominant bound vortex will cause a local increase in vortex strength, which will be transmitted either as a general small increase in the strength of the first vortex or as an earlier development with a forward movement of the whole vortex pattern; Thomson & Morrison (1969) have previously observed such axial movements. Whichever happens, the effective increase in the out-of-plane force at stations further aft will be relatively small, thus explaining the absence of major positive fluctuations on figure 12. While we believe that the description just

given of the influence of free-stream vortices is generally correct, it is of course oversimplified: for example, it should be realized that the real eddies will not produce discontinuous changes in circulation and that the surrounding flow will tend to restore the existing flow pattern as the effect of the eddy is convected along the body. This behaviour accounts for the cases to be seen on figure 13 where the pressure drops rapidly towards the mirror-image value but recovers without reaching it.

It can be seen from (3) that the ratio K_D/K_m is very sensitive to inclination. At 50° inclination, for example, the frequency of significant local disturbances at a point where $C_{of} = 0{\cdot}75$ is very low indeed, only approximately 2×10^{-9} s^{-1}. The frequency of disturbances transmitted from the region of developing asymmetry has also dropped, to 0·3 s^{-1}. This is consistent with the experimental observation of a reduced level of disturbance at higher inclinations.

The other major characteristic of the fluctuations at higher inclinations is the existence of complete switches in flow pattern, rather than temporary excursions out of the preferred state. This can be explained by the greater proportion of the out-of-plane force distribution which can be covered by a single eddy at the higher angles, where the axial length of the flow develpoment is compressed. It seems reasonable to suppose that an eddy which affects a substantial part of the development region will be capable of producing a complete switch of the whole flow pattern. The traces suggest that, once switched, the flow does not return to its original state immediately after the disturbing eddy has passed. At low angles, on the other hand, the axial extent of the eddies is too small to produce complete switches and so the original state is restored by the action of the neighbouring flow.

At very high inclinations (above 70°), switching is even more frequent. In addition to the further reduction in the spacing of the flow pattern, additional disturbances appear to be transmitted forwards along the body from the region of alternate vortex shedding which occurs at the rear of the body at these inclinations.

Equation (3) enables some comment to be made on the different time-averaged results likely to be encountered in different wind tunnels. The main variable will be turbulence intensity. Now the probability density function is highly nonlinear and a reduction in the turbulence intensity can have a strong effect on the frequency of occurrence of serious disturbances. For example, in the case at 30° incidence which was considered earlier, a reduction of the turbulence intensity by one half results in a drop in the estimated frequency of transmitted disturbances from 25·3 s^{-1} to 3·5 s^{-1}. Now many wind tunnels will have turbulence intensities much lower than the value of 0·7 % of the tunnel used in these tests. It seems therefore that other experimenters are less likely to be troubled by unsteadiness than we were. Some corroboration of this may be found in the only comparable tests, which were carried out by Bostock (1972) on a 127 mm diameter cylinder with a $2{\cdot}5R$ ellipsoidal nose. The turbulence intensity of Bostock's tunnel was 0·01 %, for which we would anticipate very little unsteadiness and therefore a higher time-averaged out-of-plane force coefficient. This is the case since Bostock reports a value of 0·8 for $\hat{C}_{of1}$ at 30° inclination,

which is identical with our predicted maximum sustainable level on the most closely comparable nose, the $2R$ ogive, and higher than our time-averaged value of 0·4 with that nose.

One aspect of the unsteadiness which is difficult to explain satisfactorily is its variability with roll angle (see §5.2.1). It is not difficult to see that small differences in geometry can determine which of the two possible states is preferred and that, since the geometry will vary with roll angle, so will the preferred state. Such geometric effects may also result in differences in the asymmetric flow development and hence in differences in susceptibility to switching by free-stream vorticity. These differences will in turn result in differing levels of unsteadiness and hence cause the time-averaged force to become dependent on the roll angle. However, it is difficult to understand how this mechanism can result in differences in the time-averaged force as large as those which were reported in §4 and which can be seen in figures 9 and 10. A more detailed study of the time-dependent behaviour may clear up this point.

6. Further discussion of the results

In §4 the time-averaged results were described and interpreted as far as was possible without knowledge of the nature of the unsteadiness. In §5, the fluctuating nature of the flow was studied and some estimates of the maximum sustainable out-of-plane force were made. This maximum sustainable force corresponds to the flow pattern remaining in one of its two possible states and therefore is the time-averaged force which would be measured in the absence of free-stream disturbances. In this section, the results of all the tests described previously are used in order to deduce the behaviour of the maximum sustainable out-of-plane force; the reasons for this behaviour are discussed with the aid of the impulsively started analogy.

6.1. *Force distribution*

The evidence of the previous two sections shows that the distributions of out-of-plane force with distance along the axis which were obtained in the time-averaged tests are of the same form as those of the maximum sustainable force; it also shows that the time-averaged tests give the correct spacings in the distribution but underestimate the amplitudes by an amount which depends on the unsteadiness.

6.1.1. *Variation of spacing.* It was pointed out in §4 that the positions $\bar{l}_C$ of the first node point for a Reynolds number of $1{\cdot}1 \times 10^5$ and angles of inclination up to 70° vary linearly with $\tan \alpha$ (see figure 4). The values of $\bar{l}_C$ from all the experiments performed with the $4R$ ogive nose are shown in figure 15. It can be seen that, at each Reynolds number, the values follow the same straight line up to an angle which depends on the Reynolds number and are constant thereafter or fall slightly. The results for the other ogive nose shapes show the same behaviour: they follow the same straight line at low angles with only slightly less accuracy than the $4R$ results and again reach a roughly constant value

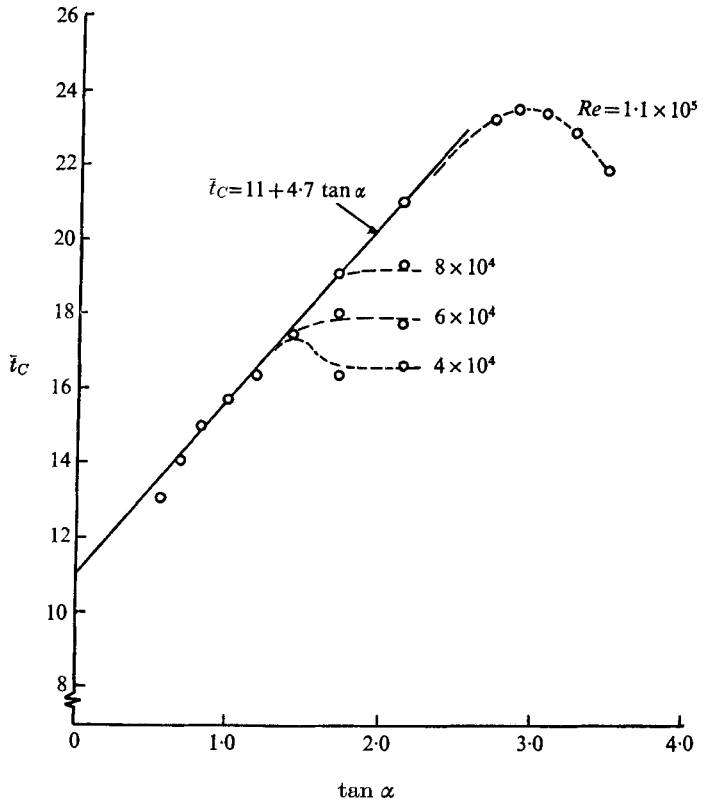

FIGURE 15. Variation of first node point with angle of inclination for the $4R$ ogive nose at various Reynolds numbers.

$\bar{l}_{C\,\mathrm{const}}$. The values of $\bar{l}_{C\,\mathrm{const}}$ are plotted aginst the nose fineness ratio F_N (the ratio of nose length to body radius) in figure 16 for two values of the Reynolds number. It can be seen that $\bar{l}_{C\,\mathrm{const}}$ decreases linearly with increasing fineness ratio at both Reynolds numbers. It can also be seen that the linear variation of $\bar{l}_{C\,\mathrm{const}}$ at the lower Reynolds number extrapolates back to the impulsively started value at zero fineness ratio. This agreement with the impulsively started value at zero fineness ratio is physically reasonable because, strictly, the simple flow analogy applies only to a cylinder with no nose.

The decrease in $\bar{l}_{C\,\mathrm{const}}$ with increasing F_N can be interpreted as being caused by an acceleration in the development of the flow on the expanding nose. The precise influence of the nose is not clear, however, since while the change in the behaviour of $\bar{l}_C$ from being linear in tan α to being roughly constant always occurs after asymmetry has moved onto the nose, the amount of development of asymmetry when the change occurs varies considerably from one case to another. At the lower angles, the linear increase in $\bar{l}_C$ with tan α has the effect of moderating the increase in axial gradients with increasing α which is implied by the simple form of the analogy. This moderation could in turn be due to a transmission of information forwards along the cylinder axis which can occur

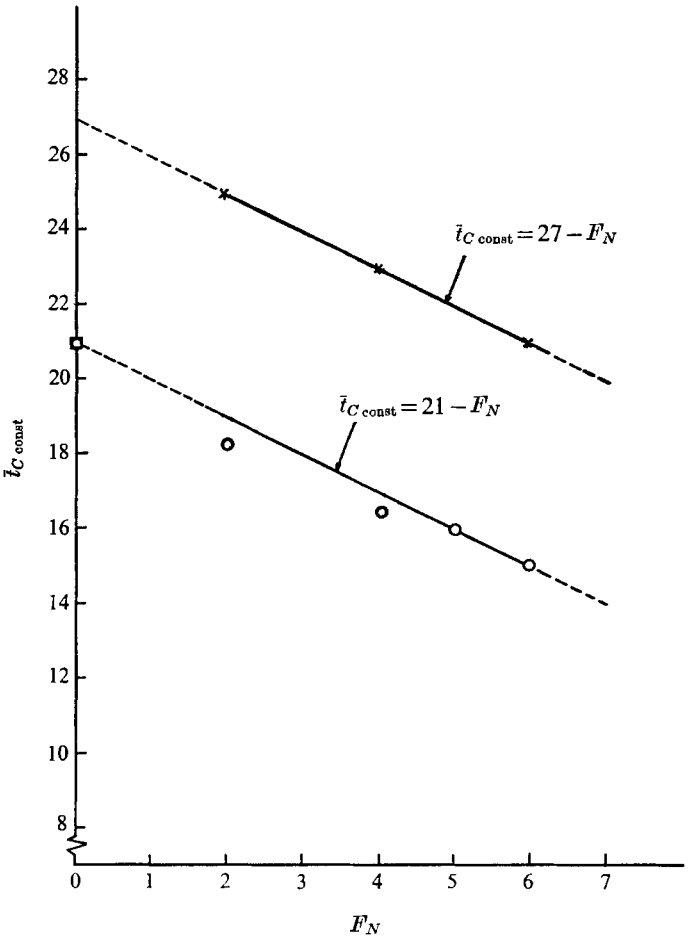

FIGURE 16. Variation of $\bar{t}_{C\,\mathrm{const}}$ with nose fineness ratio. ○, $Re = 4 \times 10^4$; ×, $Re = 1{\cdot}1 \times 10^5$; □, impulsively started value.

in the real flow but not in the analogy (where it implies a transmission of information backwards in time).

Another feature of the spacing is the onset of asymmetric flow, at point A of figure 1: we denote the value of $\bar{t}$ where this occurs as $\bar{t}_A$. In impulsively started flow, Sarpkaya (1966) found that the point A corresponds to the position of maximum drag. The results of our tests show the corresponding connexion between onset of asymmetry and maximum normal force coefficient to hold in all cases except for the $2R$ ogive nose at high angles of inclination, where the onset of asymmetry occurs slightly forward of the point of maximum normal force. The value of $\bar{t}_A$ cannot be determined from the force distributions as accurately as can $\bar{t}_C$ because of the nature of the curves in the vicinity of point A. It is difficult to discern a clear influence of inclination for a particular nose shape but it does seem that $\bar{t}_A$ decreases as the nose fineness ratio increases, particularly at the higher angles of inclination. In this respect, the behaviour is

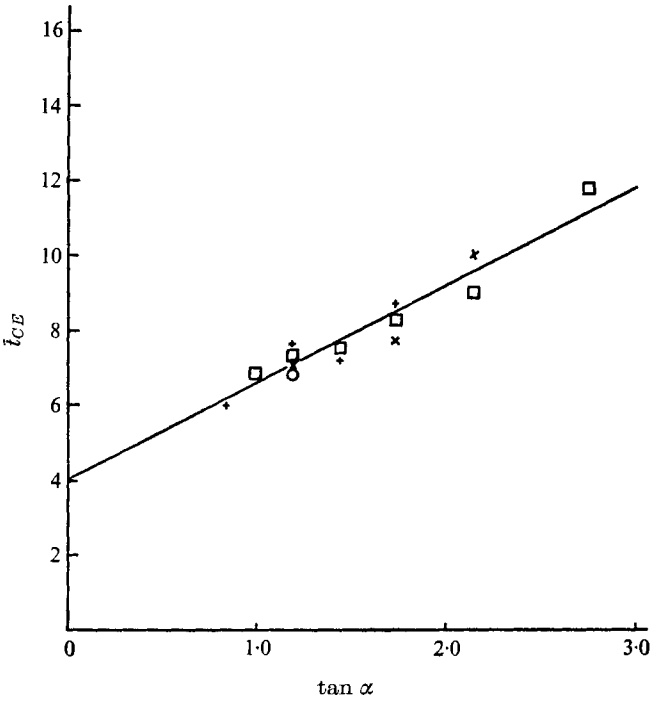

FIGURE 17. Variation of $\bar{l}_{CE}$ with inclination. ○, $2R$ ogive; □, $4R$ ogive; ×, $5R$, ogive; +, $6R$ ogive. ——, $\bar{l}_{CE} = 4 + 2{\cdot}6 \tan \alpha$.

similar to that of $\bar{l}_C$ and may also be due to an increased rate of development of the flow pattern produced by the nose.

The spacing between the node points of the second vortex shedding will be denoted by $\bar{l}_{CE}$ (see figure 1). The results from all the ogive noses are presented in figure 17; they are again roughly linear in tan α, the line shown being

$$\bar{l}_{CE} = 4 + 2{\cdot}6 \tan \alpha.$$

This may be compared to the constant value of 5 suggested by the impulsively started flow analogy. The half-period of the third vortex shedding is more difficult to estimate but appears to be roughly equal to $\bar{l}_{CE}$. The behaviour of $\bar{l}_{CE}$ is consistent with the tentative explanation given earlier for the variation of $\bar{l}_C$. Thus it shows the same increase with tan α, consistent with the moderation of the axial gradients, but does not show any significant dependence on the nose fineness ratio since this part of the flow is always on the afterbody.

6.1.2. *Peak lift coefficients.* Figures 18(*a*) and (*b*) show values of $\hat{C}_{of1}$, the maximum out-of-plane force coefficient associated with the first vortex shedding, plotted against α for the $4R$ and $6R$ ogive noses respectively. The values shown are the largest values measured at each angle and therefore correspond to a Reynolds number of 4×10^4 at the higher angles. The results from the time-dependent tests should give the most reliable estimates of the maximum sustainable force but values are also included from the time-averaged tests because the wider range of inclinations covered in these tests provides a more complete

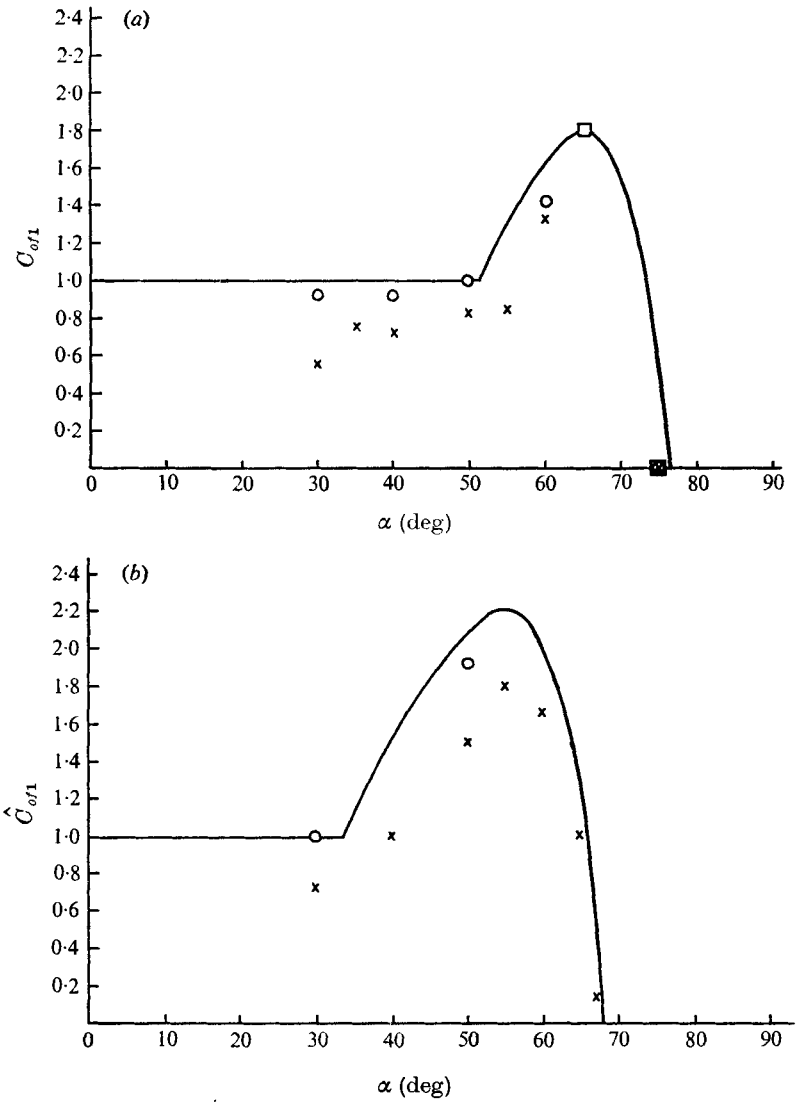

FIGURE 18. Variation of C_{of1} with inclination for (*a*) the $4R$ and (*b*) the $6R$ ogive nose. ——, estimated maximum sustainable value; ○, time-dependent test; ×, time-averaged test; □, implied from overall force measurements.

picture of the variation with inclination. Also shown are simple estimates of the variation of the maximum sustainable $\hat{C}_{of1}$. These may be thought to be rather bold considering the points shown. However, they also take account of ideas about the influence of the nose which are described in the next paragraph.

At low angles of inclination, the onset of asymmetry occurs on the constant-diameter afterbody and the results from all the nose shapes indicate a common value for $\hat{C}_{of1}$ of approximately unity. Once asymmetry moves onto the nose, $\hat{C}_{of1}$ starts to rise. The value of α where this increase begins is given by $F_N \tan \alpha = \bar{l}_A$ and differs from one nose to another since both F_N and $\bar{l}_A$ differ.

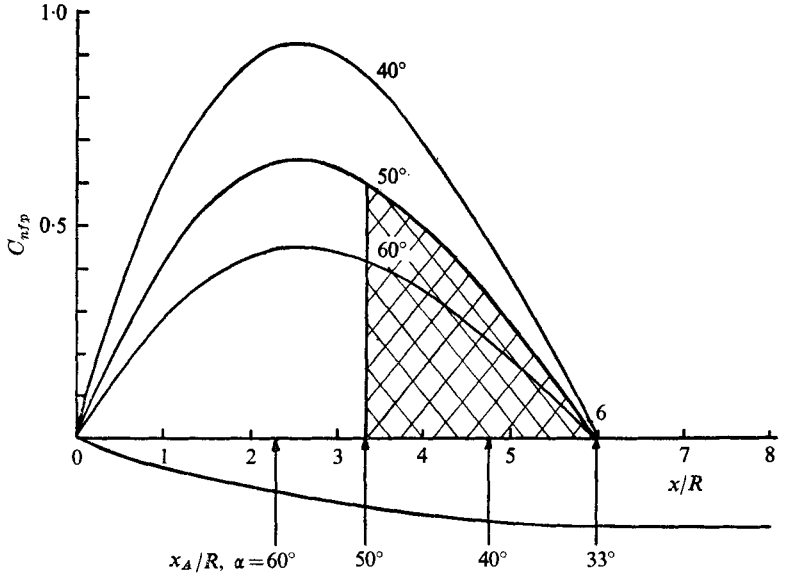

FIGURE 19. Potential-flow normal force distributions on the $6R$ ogive nose.

A maximum value of $\hat{C}_{of1}$ is attained and its value then falls to zero when sufficiently high angles are reached. The maximum value of $\hat{C}_{of1}$ depends on the nose shape; it can also depend on the Reynolds number if the maximum occurs at an angle of inclination greater than 55°.

The influence of the Reynolds number on the values of $\hat{C}_{of1}$ will be discussed in §6.2. Here we consider further the influence of the nose. Now, the evidence from the force distributions is that the level of the out-of-plane force increases when asymmetric flow occurs on the nose. This suggests that the strength of a vortex is increased when it develops on the nose. Some idea of how this can occur can be obtained from the impulsively started cross-flow analogy. According to the analogy, the nose will appear in the cross-flow plane as an expanding circular cylinder, the pressure on the windward side of the cylinder will be higher than the cross-flow total pressure and the flow will accelerate more rapidly than on a constant-diameter cylinder with the result that the amount of vorticity in the boundary layer at separation will be greater. This vorticity will in turn be fed into the developing, trapped vortex and provides a mechanism by which the increase in vortex strength can be achieved. This explanation is, of course, merely an outline and more details are needed before any serious attempt to quantify the effect directly can be made. It does, however, suggest the following simple motion. The features of the flow over the expanding cylinder which give rise to this increased vorticity are also responsible for an in-plane normal force in potential flow. The corresponding local normal force coefficient C_{nfp} is therefore likely to be related to the local effect of the nose on the out-of-plane force. Similarly, the integral of C_{nfp} (which we will call C) over the length of the first vortex is likely to be an approximate measure of the total effect of the nose on the out-of-plane force.

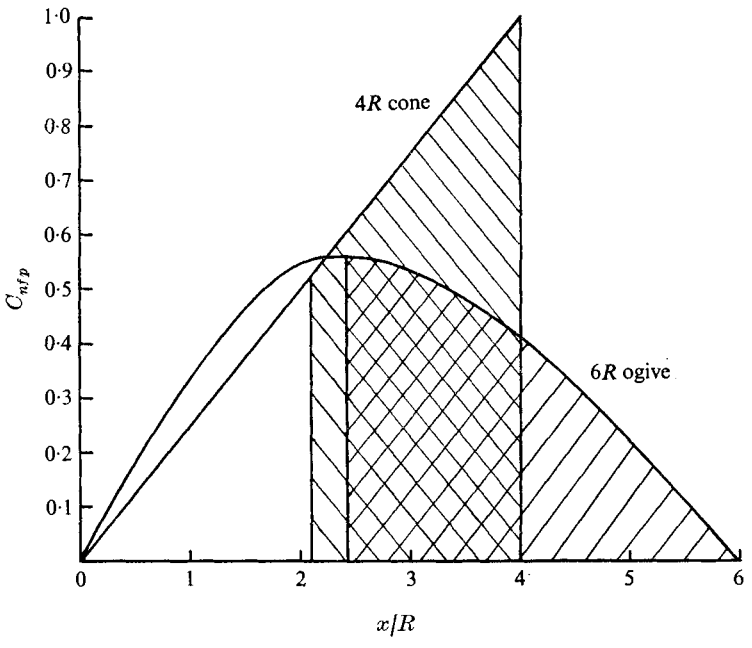

FIGURE 20. Potential-flow normal force distributions on the $6R$ ogive nose and on the $4R$ cone nose for $\alpha = 55°$.

The variation of C_{nfp} over the $6R$ nose at three inclinations was calculated by the method described by Bostock (1972) and is shown in figure 19. Also shown is the nose shape and estimates of the position of initial asymmetry (point A) at various angles of inclination. The integral quantity C at 50° inclination is the cross-hatched area on figure 19. Evaluating the integral shows that the variation of C on the $6R$ nose is similar to the variation of $\hat{C}_{of1}$. It is constant (at a value of zero) until asymmetric flow starts on the nose at 33°. Thereafter, the point of initial asymmetry advances towards the apex and C rises until the shedding point of the first vortex reaches the junction of the nose with the cylinder. This occurs at an inclination of 55°. After this point, C decreases. The accompanying fall in out-of-plane force coefficients which is observed at high angles is due not only to the effects which reduce C but also to a rapid increase in axial gradients which results in a breakdown of the flow pattern and the eventual disappearance of the out-of-plane force (this is discussed in more detail in the next sub-section).

In the case of the $4R$ nose, C again behaves in a manner consistent with the out-of-plane force coefficients. C is zero until α reaches approximately 51°, when asymmetric flow starts to occur on the nose. C then rises with α to a maximum when α is 65° and subsequently falls. Furthermore, the maximum value of C turns out to be 0·45 for the $4R$ ogive nose compared with 1·0 for the $6R$ ogive; in keeping with these values, the maximum value of $\hat{C}_{of1}$ is 1·8 on the $4R$ ogive compared with 2·2 on the $6R$ ogive. Finally, a comparison can be made between the results for the $6R$ ogive nose at 55° inclination and those for the

$4R$ conical nose at the same inclination. In both of these cases, this inclination corresponds approximately to the angle where the maximum value of $\hat{C}_{of1}$ occurs and where the whole of the growth of the first vortex occurs on the nose. The distributions of C_{nfp} are compared on figure 20. The values of C are given by the shaded areas under the curves, which are 1·4 for the conical nose and 1·0 for the $6R$ ogive. Hence the value of $\hat{C}_{of1}$ should be greater for the $4R$ cone nose than for the $6R$ ogive. Comparable time-averaged results are 2·02 and 1·75 respectively.

The evidence which has just been presented demonstrates the importance of nose shape and suggests that it may be possible to develop a simple, approximate method of prediction. However, before this can be pursued further, pressure measurements taken directly on the nose are needed. It is also worth noting that the observed changes in peak force coefficient do not necessarily represent a breakdown in the impulsively started flow analogy: it seems quite likely that, if the effect of the expanding nose could be included in the analogy, then the increased forces would be predicted. At present this cannot be done since no data exist for the lift on an expanding cylinder in impulsively started flow.

6.1.3. *Decay of out-of-plane force.* A significant difference between the out-of-plane force distribution predicted by the impulsively started flow analogy (see figure 1) and the one found in practice is that the amplitude of the real force decays to zero after only three or four half-cycles. Now, the time-dependent measurements in the region of zero average force showed a vortex-shedding region comparable to that on a yawed cylinder spanning the tunnel. The decay therefore represents the transition between the developing flow over the nose and near afterbody and the fully developed flow over an infinite cylinder. For this transitional behaviour to occur, information must be transmitted from the fully developed vortex-shedding region to regions nearer the nose. In the impulsively started analogy, this would require the transmission of information backwards in the time and is therefore not possible, thus explaining why the decay is not predicted by the analogy. Further, according to this idea, it might be expected that if the inviscid axial velocity component were supersonic then the real flow would follow the impulsively started analogy over a greater number of cycles. This is confirmed by the work of Thomson & Morrison (1969), who have shown by schlieren photography that as many as eight vortices may be shed, rather than the three or four implied in our tests. They also demonstrated that the spacing of the later vortices corresponds closely to the vortex-shedding frequency of an established Kármán vortex street.

6.2. *The effect of Reynolds number*

Evidence was presented in §§4 and 5 that a reduction in Reynolds number at angles of inclination above 55° produces a change in spacing and an increase in the out-of-plane force for all nose shapes. The effect of the Reynolds number on the peak coefficient $\hat{C}_{of1}$ is illustrated at 60° inclination for the $4R$ ogive nose in figure 21. These results were obtained in the time-averaged tests and are therefore subject to uncertainty concerning transient effects in the flow. How-

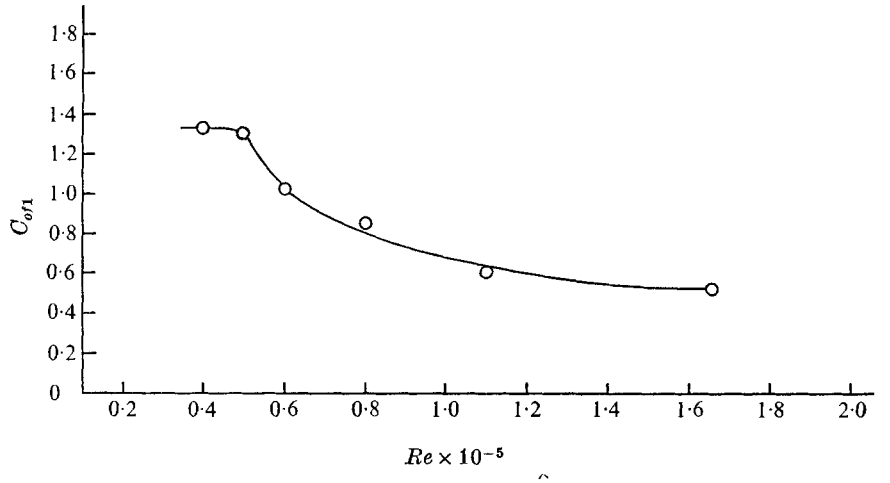

FIGURE 21. Variation of time-averaged values of $\hat{C}_{of1}$ with Reynolds number for the $4R$ ogive nose on the 51 mm diameter model at 60° inclination.

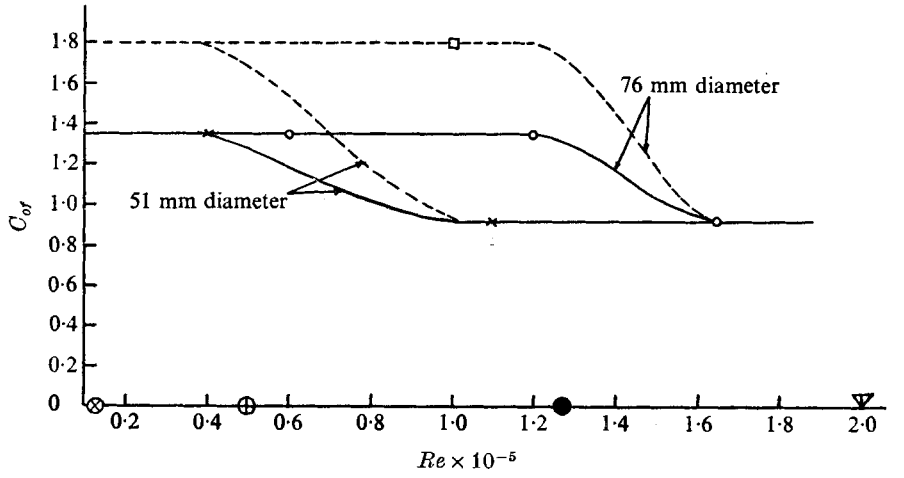

FIGURE 22. Effect of model scale on the variation of the unswitched value of C_{of} with Reynolds number for the $4R$ ogive nose at 65° inclination. ——, suggested variation at $x/R = 5$; - - - - -, suggested variation of $\hat{C}_{of1}$; ×, 51 mm model at $x/R = 5$; ○, 76 mm model at $x/R = 5$; □, implied value from overall force on 76 mm model; ▽, critical Reynolds number for transition. Lower limits of random variation of amplitude for an infinite perpendicular cylinder according to Gerrard (1961); ⊗, 6 mm diameter; ⊕, 25 mm diameter; ●, 76 mm diameter.

ever, the general validity of the trend was demonstrated by the time-dependent tests reported in § 5.

This appears to suggest a straightforward Reynolds number effect occurring at these relatively high angles. However, the results of Lamont & Hunt (1973) for the overall force on a cylinder with a $4R$ ogive nose imply that the high value of $\hat{C}_{of1}$ of 1·8 is achieved at a Reynolds number of 10^5. The only obvious difference between the overall-force model and the pressure-plotted model is

their diameters, which are 76 and 51 mm respectively. Two checks were made on this curious discrepancy. First the pressure distributions obtained at a Reynolds number of 4×10^4 on the smaller model at inclinations of 60° and 65° were integrated to give overall-force coefficients. Both gave values of about 2·5, in agreement with the upper limit of those measured in the overall-force tests and suggesting that the pressure distribution on the larger model at a Reynolds number of 10^5 is similar to that on the smaller model at a Reynolds number of 4×10^4. Second, and more conclusive, a scaled-up version of the time-dependent measuring section described in § 5 was made and fitted to the 76 mm diameter model. Time-dependent tests using this measuring section confirmed that large values of $\hat{C}_{of1}$ and an associated reduced value of $\bar{t}_C$ could be measured up to a Reynolds number of $1{\cdot}2 \times 10^5$. The difference between the results with the two cylinders can be illustrated by the values obtained from the time-dependent tests on both models at 65° inclination. These results are presented in figure 22; the values of C_{of} were recorded at station 1 ($x/R = 5$) in all cases. Note that the flow was subcritical in all these tests since the critical Reynolds number was found to be approximately 2×10^5; see § 3. Lines representing the probable variations are drawn in. Before commenting further, it should be pointed out that the comparison of levels of the lift coefficient shown in figure 22 is a little misleading since the difference in the spacing between the results for the higher and lower Reynolds number means that the lower level of C_{of} corresponds to the peak value $\hat{C}_{of1}$, whereas the upper level is a value of C_{of} below the maximum value. Making use of time-averaged values, the values of $\hat{C}_{of1}$ can be inferred at the upper level and are shown dashed on figure 22. It can be seen that the estimated upper level is consistent with the value of $\hat{C}_{of1}$ implied by the overall-force tests conducted earlier.

These differences in amplitude and spacing between tests with models of different diameter at the same Reynolds number appear to conflict with the principle of flow similarity. However, a similar situation occurs in the two-dimensional flow over a cylinder normal to the stream. Gerrard (1961) found that, at high laminar Reynolds numbers, the peak value of the fluctuating lift on the cylinder changed from a steady level to vary randomly between two extreme values. This behaviour has also been reported by Drescher (1956). In addition, Gerrard found that this behaviour occurred at a progressively lower Reynolds number as the cylinder diameter was reduced from 3 to 0·25 in. The Reynolds numbers at which this behaviour began are shown on figure 22 for three model sizes. Note the similarity of the critical model scales. Gerrard offered no explanation for this behaviour. However, it is presumably due to a change in the ratio of model scale to free-stream turbulence scale or to changes in turbulence intensity arising from changes in velocity at a constant model Reynolds number.

6.3. *Prediction of overall forces*

The results presented here were used to develop a method for predicting the maximum sustainable values of the overall out-of-plane force on ogive-nosed circular cylinders in laminar flow. Empirical representations of the distributions

of local out-of-plane force were generated, taking account of variations in inclination, nose fineness ratio and Reynolds number. The agreement between the predictions of this method and such relevant data as are available is good and adds confidence to the general validity of the results presented here. The details of the method may be found in Lamont (1973) and will be the subject of a future paper.

7. Pressure distributions

The results presented in this paper for the out-of-plane force and for the in-plane normal force have shown that each is distributed along the cylinder in a characteristic manner. The forms of these distributions are similar to those shown in figure 1. A study of the measured pressures shows that each point on the characteristic force distribution is associated with a particular shape of circumferential pressure distribution. This section presents the experimentally determined pressure distributions which occur at various points on the characteristic force curve: the points chosen are shown in figure 1. The pressure distributions are compared with distributions which occur at corresponding instants during Kármán vortex shedding. These comparisons illustrate further the relation between the variation with time in the flow over a perpendicular cylinder and the variation with distance along an inclined cylinder.

The first distribution to be examined is that at point X of figure 1, where the flow about the cylinder is such that two symmetrical vortices have formed on the lee side of the cylinder. The pressure distribution at point X obtained in a test at 20° inclination with the $4R$ ogive nose is plotted in figure 23. The pressure coefficient C_p is based on cross-flow dynamic head. On this figure, the distribution is compared with the inviscid distribution from which it has developed by the action of viscosity. It can be seen that the pressure distribution is still quite close to that of the inviscid flow The pressure distribution at the onset of asymmetry, point A, which is in addition the position of the maximum normal force, is also shown on this figure. Two examples are presented from tests at the same inclination (30°) but with different nose shapes ($4R$ and $6R$ ogives).

The next position on the characteristic out-of-plane distribution to be considered is point B. This point corresponds to the first peak value $\hat{C}_{of1}$, which occurs at the position where the first vortex is shed. Two figures, 24 and 25, are presented to show pressure distributions at point B. The former presents results for inclinations at which there is symmetric flow on the nose. The latter shows distributions for cases where the values of $\hat{C}_{of1}$ have been increased because the asymmetric flow has developed in the presence of the expanding nose pressure distribution. The other points shown on the figures are taken from Drescher's (1956) experimental results for a cylinder at 90° to the flow. They correspond to two values of the peak lift coefficient, 0·6 and 1·3, which occur at the time when a vortex is shed in the alternate vortex-shedding flow. The results from our experiments are very similar in form to those of Drescher. If they had been plotted in terms of the pressure difference between the upper

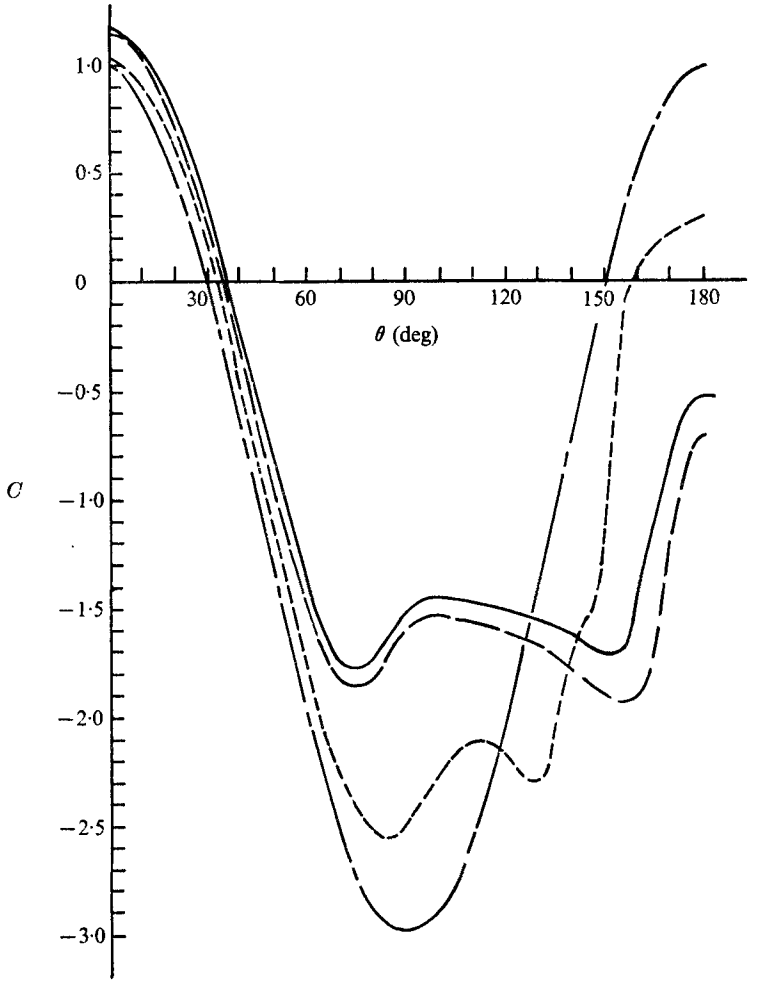

FIGURE 23. Circumferential pressure distributions. – – –, potential flow; - - - -, point X, $4R$ ogive, $\alpha = 20°$; ——, point A, $4R$ ogive, $\alpha = 30°$; – – –, point A, $6R$ ogive, $\alpha = 30°$.

and lower surface, the similarity would be even more pronounced. However, even with identical values of the out-of-plane force coefficient the distributions cannot be the same since the corresponding normal force coefficients differ. The normal force coefficient at point B is greater than the corresponding two-dimensional value, which accounts for the downward displacement of the distributions over the leeward half of the inclined cylinder. A similar situation occurs at point D, where the second vortex is shed.

Finally, three pressure distributions at points where the time-averaged out-of-plane force is zero are shown in figure 26. Two of the cases shown correspond to the point C of figure 1 while the third (called Y) is from a point where $\bar{t}$ is large and the time-averaged out-of-plane force has decayed to zero; see §6.1.3. Also shown for comparison is the time-averaged pressure distribution around a cylinder normal to the flow, as given by the *Engineering Sciences Data*

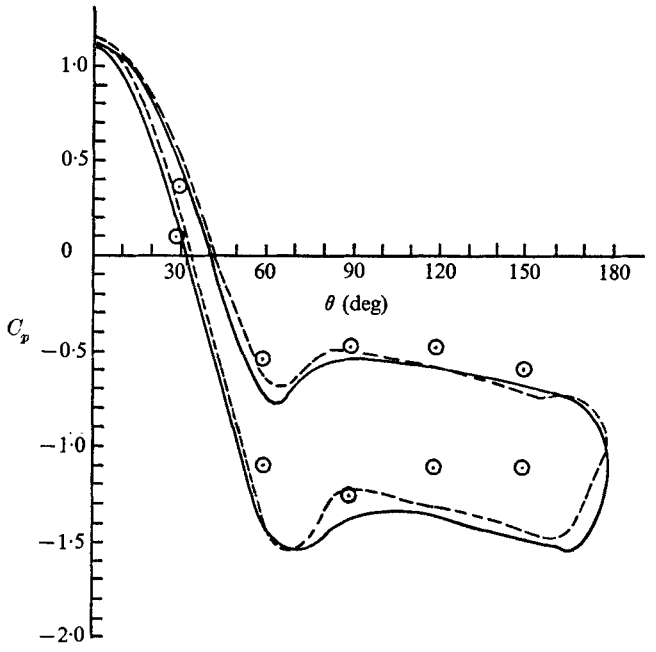

FIGURE 24. Circumferential pressure distributions at point B. ——, $4R$ ogive, $\alpha = 50°$ ($\hat{C}_{of1} = 0{\cdot}71$); – – – –, $6R$ ogive, $\alpha = 30°$ ($\hat{C}_{of1} = 0{\cdot}69$); ⊙, Drescher (1956) ($\hat{C}_{of1} \cong 0{\cdot}6$).

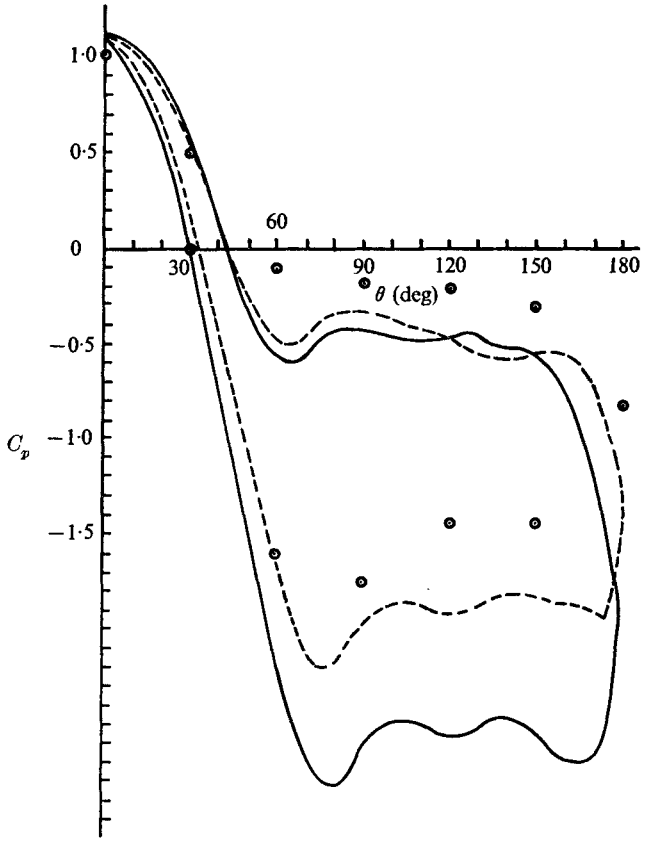

FIGURE 25. Circumferential pressure distributions at point B with asymmetric flow on the nose. ——, $6R$ ogive, $\alpha = 55°$ ($\hat{C}_{of1} = 1{\cdot}75$, $C_{nf} = 1{\cdot}7$); – – –, $4R$ ogive, $\alpha = 60°$ ($\hat{C}_{of1} = 1.3$, $C_{nf} = 1{\cdot}33$); ⊙, Drescher (1956) ($\hat{C}_{of1} = 1{\cdot}3$, $C_{nf} \cong 1{\cdot}25$).

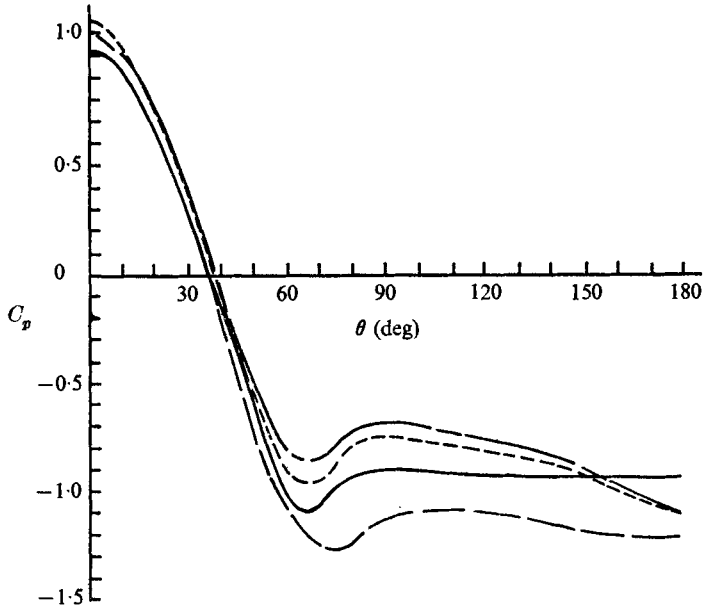

FIGURE 26. Circumferential pressure distributions. - - - point C, $4R$ ogive, $\alpha = 40°$ ($C_{nf} = 1{\cdot}14$); - · - · -, point C, $6R$ ogive, $\alpha = 30°$ ($C_{nf} = 1{\cdot}17$); ——, point Y, $4R$ ogive, $\alpha = 65°$ ($C_{nf} = 1{\cdot}04$); — —, perpendicular cylinder, $C_{nf} = 1{\cdot}2$.

Sheet no. 70013 for the case of laminar separation, where the drag coefficient C_D (equivalent to C_{nf}) is 1·2. In these cases, the normal force coefficients on the inclined cylinder are less than the two-dimensional equivalent, which is consistent with the higher base pressures. The general shapes of the curves are remarkably similar however.

8. Conclusions

The extensive pressure-plotting experiments performed in this work show that there is an oscillatory distribution of out-of-plane force along an inclined cylinder. This distribution is similar to that predicted by the impulsively started cross-flow analogy. However, there are a number of significant differences, which may be summarized as follows.

(i) The real distribution decays to zero amplitude after three or four half-cycles, whereas the flow analogy suggests that the oscillatory distribution will continue undiminished. It is thought that this decay is a result of information being transmitted through the flow towards the nose of the body.

(ii) The spacing of the out-of-plane force distribution when plotted against the equivalent impulsively started time parameter $\bar{t}$ shows some variation with angle of inclination. This has been ascribed to the transmission of information parallel to the axis and to the effect of the expanding nose.

(iii) At very high angles of inclination, the oscillatory distribution of the out-of-plane force disappears and is replaced by a vortex-shedding pattern like that on an infinite yawed cylinder at the same inclination.

(iv) At moderately high angles of inclination large increases in the out-of-plane force occur, particularly for the $6R$ ogive and $4R$ cone nose. This effect may not represent a failure of the impulsively started approach since the increases are due to the flow developing on the nose, which at present cannot be accounted for in prediction methods based on the impulsively started analogy.

Even though these differences exist, the analogy remains a very useful means of approaching this complex three-dimensional flow field. Indeed, the results presented here show that the analogy between development with time in one flow and development with length in the other is remarkably close.

The Reynolds number can have a major influence at inclinations above 55°. The peak out-of-plane force coefficient was reduced by as much as a half by increasing the Reynolds number by a factor of about three while maintaining laminar separation. It was also found that the range of Reynolds numbers over which this effect occurs varies with the scale of the model.

It has been shown that serious unsteadiness can occur in the flow. This unsteadiness involves a switching of the flow pattern from one of its two possible states towards and sometimes into the other state. Unsteadiness can greatly reduce the time-averaged value of the out-of-plane force. A fairly detailed explanation of how free-stream turbulence can be responsible for the main features of the unsteady behaviour has been given. The level of unsteadiness was found to vary with roll angle, thus accounting for the roll-angle dependence of time-averaged forces which was found in these and other tests. This dependence on roll angle must be due to the unsteady behaviour of the flow being very sensitive to small departures from axial symmetry.

P. J. Lamont gratefully acknowledges the financial support of the Science Research Council and the Guided Weapons Division of the British Aircraft Corporation.

REFERENCES

ALLEN, H. J. & PERKINS, E. W. 1951 *N.A.C.A. Rep.* no. 1048.

ATRAGHJI, E. G. 1967 *Nat. Res. Counc. Can. NAE Data Rep.* no. 5 × 5/0020.

BOSTOCK, B. R. 1972 Slender bodies of revolution at incidence. Ph.D. thesis, University of Cambridge.

BURSNAL, W. J. & LOFTIN, L. K. 1951 *N.A.C.A. Tech. Note*, no. 2463.

COE, P. L., CHAMBERS, J. R. & LETKO, W. 1972 *N.A.S.A. Tech. Note*, no. D-7095.

DRESCHER, H. 1956 *Z. Flugwiss.* **4**, 17.

GERRARD, J. H. 1961 *J. Fluid Mech.* **11**, 244.

JORGENSEN, L. H. & NELSON, E. R. 1975 *N.A.S.A. Tech. Memo.* no. X-3128.

LAMONT, P. J. 1973 The out-of-plane force on an ogive nosed cylinder at large angles of inclination to a uniform stream. Ph.D. thesis, University of Bristol.

LAMONT, P. J. & HUNT, B. L. 1973 *J. Roy. Aero. Soc.* **77**, 41.

MUNK, M. M. 1924 *N.A.C.A. Rep.* no. 184.

PICK, G. S. 1971 *A.I.A.A. Paper*, no. 71-570.

SARPKAYA, T. 1966 *A.I.A.A. J.* **4**, 414.

SURRY, J. & SURRY, D. 1967 *U.T.I.A. Tech. Note*, no. 116.

THOMSON, K. D. 1972 *Austr. W.R.E. Rep.* no. 782.

THOMSON, K. D. & MORRISON, D.F. 1969 *Australian WRE Rep.* no. HSA 25.

THOMSON, K. D. & MORRISON, D. F. 1971 *J. Fluid Mech.* **50**, 751.

TOWNSEND, A. A. 1956 *The Structure of Turbulent Shear Flow.* Cambridge University Press.

TUNSTALL, M. J. & HARVEY, J. K. 1968 *J. Fluid Mech.* **34**, 595.

WARDLAW, A. B. 1974 *A.I.A.A. J.* **12**, 1142.